A Multiscale Failure Model for Analysis of Thin Heterogeneous Plates

CAGLAR OSKAY* AND GHANSHYAM PAL

Civil and Environmental Engineering Department
Vanderbilt University, Nashville, TN 37235, USA

ABSTRACT: This manuscript presents a new multiscale framework for the analysis of failure of thin heterogeneous structures. The new framework is based on the asymptotic homogenization method with multiple spatial scales, which provides a rigorous mathematical basis for bridging the microscopic scales associated with the periodic microstructure and thickness, and the macroscopic scale associated with the in-plane dimensions of the macrostructure. The proposed approach generalizes the Caillerie–Kohn–Vogelius elastostatic heterogeneous plate theory for failure analysis when subjected to static and dynamic loads. Inelastic fields are represented using the eigendeformation concept. A computationally efficient *n*-partition computational homogenization model is developed for simulation of large scale structural systems without significantly compromising on the solution accuracy. The proposed model is verified against direct 3D finite element simulations and experimental observations under static and dynamic loads.

KEY WORDS: multiscale plate model, failure analysis, composite impact, homogenization, asymptotic analysis.

INTRODUCTION

THIN STRUCTURAL SYSTEMS composed of heterogeneous materials have been increasingly used as structural components particularly for impact, blast, and crush applications, owing largely to their favorable impact resistance, energy absorption capability, specific strength, and stiffness performance. Despite widespread use of such components, efficient and accurate modeling and simulations capabilities for the prediction of failure are not yet available. There is a need for modeling and simulation tools capable of accurately representing the complex failure processes including

matrix and fiber microcracking, interface debonding, delamination, fiber microbuckling, kink banding, and their interactions at the scale of the heterogeneities. From modeling point of view, accurate representation of these failure mechanisms in a computationally efficient manner remains to be a challenge. The clear choice for achieving this aim is multiscale structural modeling without resorting to direct 3D finite element modeling by full resolution of the microscopic fields. While direct finite element method (FEM) modeling has optimal accuracy, it typically exhausts available computational resources in simulation of large-scale systems.

Mathematical homogenization theory (MHT) provides a rigorous mathematical framework for analysis of heterogeneous materials. Since the formalization of its mathematical foundations in the seminal works of Benssousan et al. (1978), Sanchez-Palencia (1980), Babuska (1975), and Suquet (1987), MHT has been employed to characterize the response of heterogeneous solids undergoing inelastic deformations (Terada and Kikuchi, 1995; Feyel and Chaboche, 2000). This theory has also been applied to thin structures for analysis of linear elastic, nonlinear elastic as well as dynamic systems. Homogenization of thin structural systems consists of asymptotic analysis in the presence of a thickness scale in addition to the scale of the periodic heterogeneity. This approach have been formalized by Caillerie (1984), and Kohn and Vogelius (1984) for plates, by Kolpakov (1991) for beams, by Trabucho and Viano (1996) for rods and by Cioranescu and Saint Jean Paulin (1999) for reticulated structures. Despite reasonable accuracy and improved efficiency compared to direct finite element analysis using full resolution of the microstructure throughout the component scale, main difficulty with MHT-based structural models remains the high cost of solving 3D microscopic boundary value problems on the representative volume element (RVE) domain to evaluate the macroscopic constitutive response. Transformation field analysis (TFA) proposed by Dvorak and Benveniste (1992) alleviates the requirement of evaluation of the microscale boundary value problem. In this approach, the equilibrium in the microscale is satisfied by evaluating fundamental solutions of the RVE in the elastic state, and representing the inelastic fields as a function of the fundamental solutions, macroscopic deformations, and a small subset of coordinate tensors. TFA-based models have been employed to represent phase damage mechanisms (Baucom and Zikry, 2003; Bahei-El-Din et al., 2004) and viscoplasticity (Michel and Suquet, 2004). More recently, Oskay and Fish (2007, 2008) proposed the eigendeformation-based homogenization method (EHM). EHM generalizes TFA to account for the interface debonding within the RVE, and it incorporates a model selection capability to adaptively regulate the model order to match the desired accuracy and efficiency requirements.

While TFA-based models have been successfully applied to multiscale solid systems, it has not been applied to model thin multiscale structures.

In this manuscript, we present a new computational homogenization model for brittle failure of thin heterogeneous plates. The present approach is a generalization of the elastic theory proposed in Caillerie (1984) and Kohn and Vogelius (1984) for thin heterogeneous plates to account for the presence of inelastic and failure processes when subjected to static and dynamic loads. The presence of damage induced inelastic processes is represented using the eigendeformation concept. Transient dynamic effects are considered using a two-scale decomposition of time, in which, the out-of-plane deformations are taken to oscillate in much smaller time scales compared to the in-plane deformations. Asymptotic analysis of the heterogeneous plate is conducted in the presence of eigendeformation fields and inertial effects, and an inelastic plate theory is obtained for failure analysis of heterogeneous structures.

This manuscript is organized as follows: the fundamental mathematical setting of the multiscale problem and the original governing equations of the thin heterogeneous system is introduced in 'Problem Setting and Governing Equations' section. In 'Generalized Mathematical Homogenization of Thin Plates with Eigenstrains' section, the generalization of the mathematical homogenization theory for thin heterogeneous solids to dynamic-inelastic regime using the eigenstrain formulation is presented. The decomposition of the original boundary value problem in a series of microscale and macroscale problems is introduced. A computationally efficient reduced-order homogenization model for thin plates is described in 'Reduced-Order Model for Thin Plates' section. Computational aspects and the implementation details of the proposed methodology are discussed in 'Computational Aspects' section. We demonstrate the capabilities of the present modeling approach in 'Numerical Verification and Validation' section. Static three-point bending beam, mesh sensitivity analysis on notched specimens subjected to uniaxial tension, and a dynamic impact of a rigid projectile on woven composite plate simulations are conducted for verification of the proposed model. A summary and a brief discussion of future work conclude the manuscript.

PROBLEM SETTING AND GOVERNING EQUATIONS

Consider a thin heterogeneous plate, $\mathcal{B} \in \mathbb{R}^3$, formed by the repetition of a RVE in two orthogonal axes, x_1 and x_2, perpendicular to the thickness direction as shown in Figure 1. The RVE, $\mathcal{Y}$, is composed of two or more constituent materials. The domain of the heterogeneous body is defined as:

$$\mathcal{B} := \left\{ \mathbf{x} \mid \mathbf{x} = (x, x_3), \, x = \{x_1, x_2\} \in \Omega, \, c_-^\zeta(x) \le x_3 \le c_+^\zeta(x) \right\} \qquad (1)$$
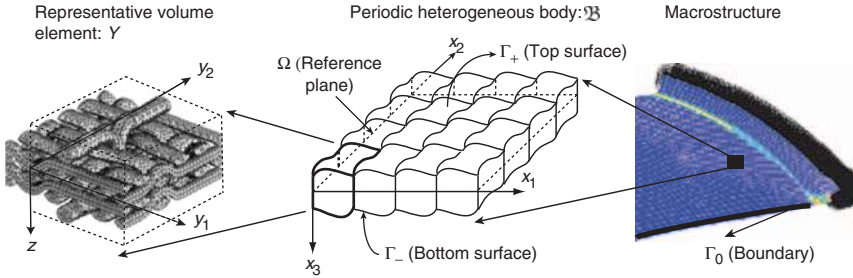
Figure 1. *Macro- and microscopic structures.*

in which, $\Omega \in \mathbb{R}^2$ is the reference surface parameterized by the Cartesian coordinate vector, x; x_3-axis denotes thickness direction; $\mathbf{x} = \{x_1, x_2, x_3\}$; $c_{\pm}^{\zeta}$ define the top $(+)$ and bottom $(-)$ boundaries of the body. Superscript ζ indicates the oscillatory characteristic of the corresponding field with a wavelength in the order of the scaling parameter ζ defined below. The Greek indices are reserved to denote 1 and 2, while lowercase Roman indices denote 1, 2, and 3.

The heterogeneity in the microconstituents properties leads to an oscillatory response, characterized by the presence of three length scales: macroscopic scale, $\mathbf{x} := \{x, x_3\}$, where $x = \{x_1, x_2\}$, associated with the overall dimensions of the macrostructure and two microscopic scales associated with the rescaled unit cell denoted by $y = \{y_1, y_2\}$, where $y = x/\zeta$, and $z = x_3/\epsilon$, associated with in-plane heterogeneity and thickness, respectively. Two scaling constants, $0 < \zeta, \epsilon \ll 1$, respectively define the ratio between the characteristic planar dimension and thickness of the RVE with respect to the deformation wavelength at the macroscopic scale. The oscillatory response is represented using a two-scale decomposition of the coordinate vector:

$$f^{\zeta\epsilon}(\mathbf{x}) = f(x, \mathbf{y}(\mathbf{x})) \qquad (2)$$

where, f denotes response fields, $\mathbf{y} := \{y, z\}$ is the microscopic coordinate vector. The spatial derivative of $f^{\zeta\epsilon}$ is calculated by the chain rule:

$$f^{\zeta\epsilon}_{,i} = \delta_{i\alpha}\left(f_{,x_\alpha} + \frac{1}{\zeta}f_{,y_\alpha}\right) + \delta_{i3}\frac{1}{\epsilon}f_{,z} \qquad (3)$$

in which, a comma followed by an index denotes derivative with respect to the components of the position vector; a comma followed by a subscript

variable x_α or y_i denotes a partial derivative with respect to the components of the macroscopic and microscopic position vectors, respectively; and δ_{ij} denotes the components of the Kronecker delta.

The RVE, $\mathcal{Y}$, is defined in terms of the microscopic coordinates:

$$\mathcal{Y} := \{\mathbf{y} \mid \mathbf{y} = (y, z), \ y = \{y_1, y_2\} \in Y, \ c^-(y) \leq z \leq c^+(y)\} \qquad (4)$$

in which $Y \in \mathbb{R}^2$ is the reference surface in the RVE. The boundaries of the RVE are defined as:

$$\Gamma_\pm^{\mathcal{Y}} = \{\mathbf{y} \mid y \in Y, \ z = c^\pm(y)\} \qquad (5)$$

$$\Gamma_{\text{per}}^{\mathcal{Y}} = \{\mathbf{y} \mid y \in \partial Y, \ c^-(y) < z < c^+(y)\} \qquad (6)$$

The boundary functions, $c^\pm$ are scaled with respect to the corresponding functions in the original single scale coordinate system: $c_\pm^\zeta(x) = \epsilon c^\pm(y)$.

Remark 1:

   We consider the following restrictions on the response fields:

   – All fields are assumed to be periodic in the microscopic planar directions:

$$f(x, y, z) = f(x, y + k\hat{y}, z)$$

   where, $\hat{y}$ denotes the periods of the microstructure; and k is a diagonal matrix with integer components.
   – The structure is taken to be thin throughout (i.e., $c_+^\zeta - c_-^\zeta = O(\epsilon)$).
   – The thickness and the planar dimensions of the RVE is of the same order of magnitude ($\epsilon = O(\zeta)$). By this restriction, one of the scaling parameters is eliminated and the formulation includes a single scaling parameter. Alternative formulations for tall reticulated structures (i.e., $\epsilon \gg \zeta$), and plates with moderate heterogeneities in the planar directions (i.e., $\zeta \gg \epsilon$) have been previously considered by other researchers (Miller, 1994; Cioranescu and Donato, 1999) in the context of elastic analysis.

Original Boundary Value Problem

   Failure of the heterogeneous body is considered as the progressive degradation of the material properties within the microconstituents when subjected to mechanical loads of sufficient amplitude. The microconstituents are assumed to be perfectly bonded along the interfaces.

The governing equations of the failure of the heterogeneous body are expressed as ($\mathbf{x} \in \mathcal{B}$, $t \in [0, t_0]$):

$$\sigma_{ij,j}^{\zeta}(\mathbf{x}, t) + b_i^{\zeta}(\mathbf{x}, t) = \rho^{\zeta}(\mathbf{x})\ddot{u}_i^{\zeta}(\mathbf{x}, t) \tag{7}$$

$$\sigma_{ij}^{\zeta}(\mathbf{x}, t) = L_{ijkl}^{\zeta}(\mathbf{x})\left[\epsilon_{kl}^{\zeta}(\mathbf{x}, t) - \mu_{kl}^{\zeta}(\mathbf{x}, t)\right] \tag{8}$$

$$\epsilon_{ij}^{\zeta}(\mathbf{x}, t) = u_{(i,j)}^{\zeta}(\mathbf{x}, t) \equiv \frac{1}{2}\left(\frac{\partial u_i^{\zeta}}{\partial x_j} + \frac{\partial u_j^{\zeta}}{\partial x_i}\right) \tag{9}$$

$$\mu_{ij}^{\zeta}(\mathbf{x}, t) = \omega^{\zeta}(\mathbf{x}, t)\epsilon_{ij}^{\zeta}(\mathbf{x}, t) \tag{10}$$

$$\omega^{\zeta}(\mathbf{x}, t) = \omega^{\zeta}\left(\sigma_{ij}^{\zeta}, \epsilon_{ij}^{\zeta}, \mathbf{s}^{\zeta}\right) \tag{11}$$

where, u_i^{ζ} denotes the components of the displacement vector; σ_{ij}^{ζ} the Cauchy stress; ϵ_{ij}^{ζ} and μ_{ij}^{ζ} the total strain and inelastic strain tensors, respectively; $\omega^{\zeta} \in [0, 1]$ is the scalar damage variable, with $\omega^{\zeta} = 0$ corresponding to the state of no damage, and $\omega^{\zeta} = 1$ denoting a complete loss of load-carrying capacity; b_i^{ζ} the body force; $\rho^{\zeta}(\mathbf{x}, t)$ density, and; t the temporal coordinate. Superposed single and double dot correspond to material time derivative of orders one and two, respectively. L_{ijkl}^{ζ}, the tensor of elastic moduli, obeys the conditions of symmetry

$$L_{ijkl}^{\zeta} = L_{jikl}^{\zeta} = L_{ijlk}^{\zeta} = L_{klij}^{\zeta} \tag{12}$$

and positivity:

$$\exists C_0 > 0; \quad L_{ijkl}^{\zeta}\xi_{ij}\xi_{kl} \geq C_0\xi_{ij}\xi_{kl} \quad \forall \xi_{ij} = \xi_{ji} \tag{13}$$

The evolution equation of ω^{ζ} is given in a functional form (Equation (11)) as a function of strain, stress, and additional state variables $\mathbf{s}^{\zeta}$. The specific form of the damage evolution within the microstructure is presented in 'Rate-dependent Damage Evolution Model' section (see Krajcinovic, 1996 for a rather complete treatise on continuous damage mechanics approach).

The initial and boundary conditions are assumed to be a function of the macroscopic coordinates only. The initial conditions are

$$u_i^{\zeta}(\mathbf{x}, t) = \hat{u}_i(\mathbf{x}); \quad \dot{u}_i^{\zeta}(\mathbf{x}, t) = \hat{v}_i(\mathbf{x}); \quad \mathbf{x} \in \mathcal{B}; \quad t = 0 \tag{14}$$

The boundary of the structure is defined by $\Gamma = \Gamma_{\pm} \cup \Gamma_0$, as illustrated in Figure 1.

$$\Gamma_{\pm} = \left\{\mathbf{x} \,|\, x \in \Omega, \, x_3 = c_{\pm}^{\zeta}(\mathbf{x})\right\} \tag{15}$$

$$\Gamma_0 = \left\{\mathbf{x} \,|\, x \in \partial\Omega, \, c_-^{\zeta}(\mathbf{x}) < x_3 < c_+^{\zeta}(\mathbf{x})\right\} \tag{16}$$

Homogeneous displacement conditions are assumed on Γ_0, whereas traction boundary conditions are assumed on $\Gamma_\pm$:

$$u_i^\zeta(\mathbf{x}, t) = 0; \quad \mathbf{x} \in \Gamma_0; \quad t \in [0, t_\mathrm{o}] \tag{17}$$

$$\sigma_{ij}^\zeta(\mathbf{x}, t)n_j = \overline{\tau}_i^\pm(\mathbf{x}, t); \quad \mathbf{x} \in \Gamma_\pm; \quad t \in [0, t_\mathrm{o}] \tag{18}$$

The above boundary conditions are chosen for simplicity of the presentation. Treatment of the general (displacement, traction, and mixed type) boundary conditions is presented in 'Boundary Conditions' section.

GENERALIZED MATHEMATICAL HOMOGENIZATION OF THIN PLATES WITH EIGENSTRAINS

We employ the mathematical homogenization theory with multiple scales to evaluate the failure of thin structural systems described by Equations (7)–(18). To this extent, we generalize the linear elastic composite thin plate theory first proposed by Caillerie (1984) and, Kohn and Vogelius (1984) to account for the presence of inelastic and damage fields using the eigendeformation concept (Oskay and Fish, 2007). We start by an asymptotic decomposition of the displacement field:

$$u_i^\zeta(\mathbf{x}, t) = \delta_{i3}w(x, t) + \zeta u_i^1(x, \mathbf{y}, t) + \zeta^2 u_i^2(x, \mathbf{y}, t) + \cdots \tag{19}$$

where, w is the out of plane displacement, and $u^1, u^2, \ldots$ denote higher order displacements. Analogous expressions have also been proposed in asymptotic analysis of heterogeneous rods (see e.g., Kolpakov, 1991; Trabucho and Viano, 1996). We further assume that the transient motion in the thickness direction is dictated by the presence of much smaller time scales ($O(\zeta^{-2})$) compared to the planar deformation:

$$u_\alpha^\zeta(\mathbf{x}, t) = u_\alpha(x, \mathbf{y}, t) \tag{20}$$

$$u_3^\zeta(\mathbf{x}, t) = u_3(x, \mathbf{y}, \zeta^2 t) \tag{21}$$

This condition ensures recovery of the classical plate theory in the static limit. Similar scalings have been used in the context of plate dynamics (e.g., Tarn and Wang, 1994).

The damage variable is approximated as

$$\omega^\zeta(\mathbf{x}, t) = \omega(x, \mathbf{y}, t) + O(\zeta) \tag{22}$$

The following load scalings are necessary to account for the diminishing transverse dimensions of the heterogeneous structure (Lewinski and Telega, 2000):

$$b_\alpha^\zeta(\mathbf{x}, t) = \zeta b_\alpha(x, \mathbf{y}, t); \quad b_3^\zeta(\mathbf{x}, t) = \zeta^2 b_3(x, \mathbf{y}, t) \tag{23a}$$

$$\bar{\tau}_\alpha^\pm(\mathbf{x}, t) = \zeta^2 \bar{p}_\alpha^\pm(x, t); \quad \bar{\tau}_3^\pm(\mathbf{x}, t) = \zeta^3 \bar{q}^\pm(x, t) \tag{23b}$$

$$\rho^\zeta(\mathbf{x}) = \rho(\mathbf{y}) \tag{23c}$$

The strain field is expressed in terms of an asymptotic series by using the chain rule (Equation (3)) as well as Equations (9) and (19):

$$\epsilon_{ij}^\zeta(\mathbf{x}, t) = \sum_{\eta=0}^\infty \zeta^\eta \epsilon_{ij}^\eta(x, \mathbf{y}, t) \tag{24}$$

where the components of the strain field are expressed as:

$$\epsilon_{\alpha\beta}^0(x, \mathbf{y}, t) = u_{(\alpha, y_\beta)}^1; \quad \epsilon_{\alpha 3}^0(x, \mathbf{y}, t) = \frac{1}{2} w_{,x_\alpha} + u_{(3, y_\alpha)}^1; \quad \epsilon_{33}^0(x, \mathbf{y}, t) = u_{3,z}^1 \quad \text{(25a)}$$

$$\epsilon_{\alpha\beta}^\eta(x, \mathbf{y}, t) = u_{(\alpha, x_\beta)}^\eta + u_{(\alpha, y_\beta)}^{\eta+1}; \quad \epsilon_{3\alpha}^\eta(x, \mathbf{y}, t) = \frac{1}{2} u_{3, x_\alpha}^\eta + u_{(3, y_\alpha)}^{\eta+1};$$

$$\epsilon_{33}^1(x, \mathbf{y}, t) = u_{3,z}^{\eta+1} \tag{25b}$$

$\eta = 1, 2, \ldots$

The stress field is also expressed based on asymptotic expansion:

$$\sigma_{ij}^\zeta(\mathbf{x}, t) = \sum_{\eta=0}^\infty \zeta^\eta \sigma_{ij}^\eta(x, \mathbf{y}, t) \tag{26}$$

using Equations (8), (22) and (24), the components of the stress field are obtained:

$$\sigma_{ij}^\eta(x, \mathbf{y}, t) = L_{ijkl}(\mathbf{y})\left[\epsilon_{kl}^\eta(x, \mathbf{y}, t) - \mu_{kl}^\eta(x, \mathbf{y}, t)\right] \tag{27}$$

where,

$$\mu_{kl}^\eta = \omega(x, \mathbf{y}, t)\epsilon_{ij}^\eta(x, \mathbf{y}, t) \tag{28}$$

The momentum balance equations in various orders are obtained by substituting Equations (19) and (26) into Equation (7), and using Equations (20), (21) and (23):

$$O(\zeta^{-1}) \quad : \quad \sigma^0_{ij,y_j} = 0 \tag{29a}$$

$$O(1) \quad : \quad \sigma^0_{i\alpha,x_\alpha} + \sigma^1_{ij,y_j} = 0 \tag{29b}$$

$$O(\zeta) \quad : \quad \sigma^1_{i\alpha,x_\alpha} + \sigma^2_{ij,y_j} + \delta_{i\alpha}b_\alpha = \delta_{i\alpha}\rho\ddot{u}^1_\alpha \tag{29c}$$

$$O(\zeta^2) \quad : \quad \sigma^2_{i\alpha,x_\alpha} + \sigma^3_{ij,y_j} + \delta_{i3}b_3 = \delta_{i\alpha}\rho\ddot{u}^2_\alpha + \delta_{3i}\rho\ddot{w} \tag{29d}$$

$$O(\zeta^\eta) \quad : \quad \sigma^\eta_{i\alpha,x_\alpha} + \sigma^{\eta+1}_{ij,y_j} = \delta_{i\alpha}\rho\ddot{u}^\eta_\alpha + \delta_{3i}\rho\ddot{u}^{\eta-2}_3, \quad \eta = 3,4,\ldots \tag{29e}$$

Similarly, substituting stress and displacement decompositions (Equations (19) and (26)) into Equations (17) and (18), and using Equation (23b) gives the boundary conditions in various orders:

$$O(1) \quad : \quad \sigma^0_{ij}(x,\mathbf{y},t)n_j = 0, \quad x \in \Gamma_\pm; \qquad w(x,t) = 0, \quad x \in \Gamma_0 \tag{30a}$$

$$O(\zeta) \quad : \quad \sigma^1_{ij}(x,\mathbf{y},t)n_j = 0, \quad x \in \Gamma_\pm; \qquad u^1_i(x,\mathbf{y},t) = 0, \quad x \in \Gamma_0 \tag{30b}$$

$$O(\zeta^2) \quad : \quad \sigma^2_{ij}(x,\mathbf{y},t)n_j = \delta_{i\alpha}\overline{\tau}^\pm_\alpha(x), \quad x \in \Gamma_\pm; \quad u^2_i(x,\mathbf{y},t) = 0, \quad x \in \Gamma_0 \tag{30c}$$

$$O(\zeta^3) \quad : \quad \sigma^3_{ij}(x,\mathbf{y},t)n_j = \delta_{i3}\overline{\tau}^\pm_3(x), \quad x \in \Gamma_\pm; \quad u^3_i(x,\mathbf{y},t) = 0, \quad x \in \Gamma_0 \tag{30d}$$

$$O(\zeta^\eta) \quad : \quad \sigma^\eta_{ij}(x,\mathbf{y},t)n_j = 0, \quad x \in \Gamma_\pm; \qquad u^\eta_i(x,\mathbf{y},t) = 0, \quad x \in \Gamma_0 \tag{30e}$$
$$\eta = 4,5,\ldots$$

First-order Microscale Problem

The $O(\zeta^{-1})$ equilibrium equation along with the $O(1)$ constitutive and kinematic equations, and initial and boundary conditions form the first-order microscale problem (RVE[1]). RVE[1] is summarized in Box 1. In what follows, we formulate the evolution of microscale problems based on transformation field analysis.

For a fixed macroscopic state and time (i.e., evolution of the system is frozen), the eigendeformation concept may be invoked to evaluate the first-order microscale problem. By this approach, $w_{,x_\alpha}$ and μ^0_{kl} are viewed as forces acting on an instantaneously linear system. Hence, the microscopic displacement field is decomposed as:

$$u^1_i(x,\mathbf{y},t) = u^{1w}_i(x,\mathbf{y},t) + u^{1\mu}_i(x,\mathbf{y},t) \tag{31}$$

Given: material properties, $L_{ijkl}(\mathbf{y})$, macroscopic strains, $w_{,x_\alpha}$, and the inelastic strain field, μ_{kl}^0

Find: for a fixed $\overline{x} \in \Omega$ and $\overline{t} \in [0, t_0]$, the microscopic deformations, $u_i^1(\overline{x}, \mathbf{y}, \overline{t}) \in \overline{\mathcal{Y}} \to \mathbb{R}$ which satisfy

- Equilibrium:

$$\left\{ L_{ijkl}(\mathbf{y})u_{(k,y_l)}^1(\overline{x}, \mathbf{y}, \overline{t}) + L_{ij\alpha3}(\mathbf{y})w_{,x_\alpha}(\overline{x}, \overline{t}) - L_{ijkl}(\mathbf{y})\mu_{kl}^0(\overline{x}, \mathbf{y}, \overline{t}) \right\}_{,y_j} = 0$$

- Boundary conditions:
  - $u_{(i,y_j)}^1$ periodic on $\mathbf{y} \in \Gamma_0^{\mathcal{Y}}$
  - $\{L_{ijkl}u_{(k,y_l)}^1 + L_{ij\alpha3}w_{,x_\alpha} - L_{ijkl}\mu_{kl}^0\}n_j = 0$ on $\mathbf{y} \in \Gamma_{\pm}^{\mathcal{Y}}$

Box 1: The first-order RVE problem (RVE[1]).

where, u_i^{1w} and $u_i^{1\mu}$ are displacement fields induced by the macroscopic deformation and inelastic strains, respectively. The above decomposition is valid for arbitrary damage state. We first consider the damage-free state (i.e., $\mu_{kl}^0 = 0 \to u_i^{1\mu} = 0$). At this state, the RVE[1] problem may be trivially satisfied when the microscopic displacement takes the following form:

$$u_i^1 = u_i^{1w}(x, \mathbf{y}, t) = u_i(x, t) - \hat{z}\delta_{i\alpha}w_{,x_\alpha}(x, t) \tag{32}$$

where, $\hat{z} = z - \langle z \rangle$, and; $\langle \cdot \rangle := 1/|\mathcal{Y}| \int_{\mathcal{Y}} \cdot \, d\mathcal{Y}$ denotes volume averaging on the RVE. Next, we consider the case when the macroscopic deformations vanish at an arbitrary damage state. The resulting system of equations constitutes an elasticity problem with eigenstrains, μ_{ij}^0. The solution may be expressed in terms of damage influence function, $\tilde{\Theta}_{ikl}$ as follows

$$u_i^1 = u_i^{1\mu}(x, \mathbf{y}, t) = \int_{\mathcal{Y}} \tilde{\Theta}_{ikl}(\mathbf{y}, \hat{\mathbf{y}})\mu_{kl}^0(x, \hat{\mathbf{y}}, t)d\hat{\mathbf{y}} \tag{33}$$

The damage influence function is evaluated by solving the first-order damage influence function (DIF[1]) problem defined in Box 2.

Remark 2:

The general expression for the microscopic displacement field, u_i^1 becomes

$$u_i^1(x, \mathbf{y}, t) = u_i(x, t) - \hat{z}\delta_{i\alpha}w_{,x_\alpha}(x, t) + \int_{\mathcal{Y}} \tilde{\Theta}_{ikl}(\mathbf{y}, \hat{\mathbf{y}})\mu_{kl}^0(x, \hat{\mathbf{y}}, t)d\hat{\mathbf{y}}$$

Given: material properties, $L_{ijmn}(\mathbf{y})$ and d is Dirac delta function.
Find: $\tilde{\Theta}_{ikl}(\mathbf{y}, \hat{\mathbf{y}}) : \overline{\mathcal{Y}} \times \overline{\mathcal{Y}} \to \mathbb{R}$ such that:

- Equilibrium:

$$\left\{ L_{ijmn}(\mathbf{y}) \big(\tilde{\Theta}_{(m,\, y_n)kl}(\mathbf{y}, \hat{\mathbf{y}}) + I_{mnkl} d(\mathbf{y} - \hat{\mathbf{y}}) \big) \right\}_{,\, y_j} = 0; \quad \mathbf{y}, \hat{\mathbf{y}} \in \mathcal{Y}$$

- Boundary conditions:
  - $\tilde{\Theta}_{ik\beta}$ periodic on $\mathbf{y} \in \Gamma_0^{\mathcal{y}}$
  - $L_{ijmn}(\mathbf{y}) \big(\tilde{\Theta}_{(m,\, y_n)kl}(\mathbf{y}, \hat{\mathbf{y}}) + I_{mnkl} d(\mathbf{y} - \hat{\mathbf{y}}) \big) n_j = 0$ on $\mathbf{y} \in \Gamma_\pm^{\mathcal{y}}$

Box 2: The first-order damage influence function problem (DIF[1]).

Gradient of the above equation substituted into Equations (25a) and (28) leads to

$$\mu_{ij}^0(x, \mathbf{y}, t) = \omega(x, \mathbf{y}, t) \int_{\mathcal{Y}} \tilde{\Theta}_{(i,\, y_j)kl}(\mathbf{y}, \hat{\mathbf{y}}) \mu_{kl}^0(x, \hat{\mathbf{y}}, t) \mathrm{d}\hat{\mathbf{y}}$$

The above is a homogeneous integral equation. For an arbitrary damage state, ω, it can only be satisfied trivially (Courant and Hilbert, 1989) (i.e., $\mu_{ij}^0 = 0$), and the microscopic displacement field expression reduces to Equation (32).

Second-order Microscale Problem

The $O(\zeta)$ equilibrium equation along with the $O(1)$ constitutive and kinematic equations, and initial and boundary conditions form the second-order microscale problem (RVE[2]) as summarized in Box 3.

The second-order microscale problem is evaluated analogous to the first-order problem using the eigendeformation concept. The forcing terms in RVE[2] are the macroscopic generalized strains, u_{i,x_α} and $w_{,x_\alpha}$ as well as the inelastic strains, μ_{ij} (superscript 1 is omitted in what follows for conciseness). The microscopic displacement field is evaluated by considering the following decomposition:

$$u_i^2 = u_i^{2w} + u_i^{2u} \tag{34}$$

in which, u_i^{2w} and u_i^{2u} correspond to the displacement components due to the forcing terms associated with the macroscopic displacements w

Given: material properties, $L_{ijkl}(\mathbf{y})$, macroscopic strains, $w_{,x_\alpha x_\beta}$ and u_{i,x_α}, and inelastic strain tensor, μ_{kl}

Find: for a fixed $\overline{x} \in \Omega$ and $\overline{t} \in [0, t_0]$, the microscopic displacements $u_i^2(\overline{x}, \mathbf{y}, \overline{t}) \in \overline{\mathcal{Y}} \to \mathbb{R}$ which satisfy

- Equilibrium:

$$\left\{ L_{ijkl}(\mathbf{y})u_{(k,y_l)}^2(\overline{x}, \mathbf{y}, \overline{t}) + L_{ij\alpha 3}(\mathbf{y})u_{3,x_\alpha}(\overline{x}, \overline{t}) + L_{ij\alpha\beta}(\mathbf{y}) \right.$$
$$\left. \times \left(u_{(\alpha,x_\beta)}(\overline{x}, t) - \hat{z}w_{,x_\alpha x_\beta}(\overline{x}, t) \right) - L_{ijkl}(\mathbf{y})\mu_{kl}(\overline{x}, \mathbf{y}, \overline{t}) \right\}_{,y_j} = 0$$

- Boundary conditions:
  - $u_{(i,y_j)}^2$ periodic on $\mathbf{y} \in \Gamma_0^{\mathcal{Y}}$
  - $\{ L_{ijkl}(\mathbf{y})u_{(k,y_l)}^2(\overline{x}, \mathbf{y}, \overline{t}) + L_{ij\alpha 3}(\mathbf{y})u_{3,x_\alpha}(\overline{x}, \overline{t}) + L_{ij\alpha\beta}(\mathbf{y})$
    $\times \left(u_{(\alpha,x_\beta)}(\overline{x}, t) - \hat{z}w_{,x_\alpha x_\beta}(\overline{x}, t) \right) - L_{ijkl}(\mathbf{y})\mu_{kl}(\overline{x}, \mathbf{y}, \overline{t}) \}n_j = 0$ on $\mathbf{y} \in \Gamma_\pm^{\mathcal{Y}}$

Box 3: The second-order RVE problem (RVE^2).

and u_i, respectively. First, consider the case when $w = 0$. Employing the eigendeformation concept, the microscopic displacement field is expressed in terms of the influence functions:

$$u_i^{2u}(x, \mathbf{y}, t) = \Theta_{i\alpha\beta}(\mathbf{y})u_{(\alpha,x_\beta)}(x, t) - \hat{z}\delta_{i\alpha}u_{3,x_\alpha}(x, t)$$
$$+ \int_{\mathcal{Y}} \tilde{\Theta}_{ikl}(\mathbf{y}, \hat{\mathbf{y}})\overline{\mu}_{kl}(x, \hat{\mathbf{y}}, t)\mathrm{d}\hat{\mathbf{y}} \tag{35}$$

in which, $\overline{\mu}_{k\beta}$ denotes the components of the inelastic strain field due to in-plane deformations, and; Θ_{ikl} is the first-order elastic influence function. $\Theta_{ik\beta}$ is the solution to the first-order elastic influence function problem outlined in Box 4.

Considering the case when $u_i = 0$ with nonzero w, the microscopic displacement field is expressed in terms of the second-order influence functions as

$$u_i^{2w}(x, \mathbf{y}, t) = \Xi_{i\alpha\beta}(\mathbf{y})w_{,x_\alpha x_\beta}(x, t) + \int_{\mathcal{Y}} \tilde{\Xi}_{ikl}(\mathbf{y}, \hat{\mathbf{y}})\hat{\mu}_{kl}(x, \hat{\mathbf{y}}, t)\mathrm{d}\hat{\mathbf{y}} \tag{36}$$

where, $\hat{\mu}_{ij}$ denotes the components of the inelastic strain field due to the bending deformation; $\Xi_{i\alpha\beta}$ and $\tilde{\Xi}_{ikl}$ the second-order elastic and damage

---

Given: material properties $L_{ijkl}(\mathbf{y})$.

Find: $\Theta_{i\alpha\beta}(\mathbf{y}) : \overline{\mathcal{Y}} \to \mathbb{R}$ such that:
- Equilibrium:

$$\left\{ L_{ijmn}\Theta_{(m,y_n)\alpha\beta}(\mathbf{y}) + L_{ij\alpha\beta}(\mathbf{y}) \right\}_{,y_j} = 0$$

- Boundary conditions:
  - $\Theta_{i\alpha\beta}$ periodic on $\mathbf{y} \in \Gamma_0^{\mathcal{Y}}$
  - $L_{ijmn}(\mathbf{y})\left(\Theta_{(m,y_n)\alpha\beta}(\mathbf{y}) + I_{mn\alpha\beta}(\mathbf{y})\right)n_j = 0$ on $\mathbf{y} \in \Gamma_\pm^{\mathcal{Y}}$

Box 4: The first-order elastic influence function problem (EIF[1]).

Given: material properties $L_{ijkl}(\mathbf{y})$.

Find: $\Xi_{i\alpha\beta}(\mathbf{y}) : \overline{\mathcal{Y}} \to \mathbb{R}$ such that:
- Equilibrium:

$$\left\{ L_{ijmn}\Xi_{(m,y_n)\alpha\beta}(\mathbf{y}) - \hat{z}L_{ij\alpha\beta}(\mathbf{y}) \right\}_{,y_j} = 0$$

- Boundary conditions:
  - $\Xi_{i\alpha\beta}$ periodic on $\mathbf{y} \in \Gamma_0^{\mathcal{Y}}$
  - $L_{ijmn}(\mathbf{y})\left(\Xi_{(m,y_n)\alpha\beta}(\mathbf{y}) - \hat{z}I_{mn\alpha\beta}(\mathbf{y})\right)n_j = 0$ on $\mathbf{y} \in \Gamma_\pm^{\mathcal{Y}}$

Box 5: The second-order elastic influence function problem (EIF[2]).

influence functions, respectively. $\Xi_{i\alpha\beta}$ and $\tilde{\Xi}_{ikl}$ are solutions to elastic and damage influence function problems (EIF[2]) and (DIF[2]), respectively, which are summarized in Boxes 5 and 6. Under general loading conditions (nonzero u_i and w with arbitrary damage state, ω), microscopic displacement field, u_i^2 is given by Equation (34) with the right-hand-side terms provided by Equations (35) and (36).

Remark 3:

The transverse shear stress components vanish:

$$\left\langle \sigma_{3j}^1(x, \mathbf{y}, t) \right\rangle = 0 \tag{37}$$

The stress field may be expressed in terms of the influence functions by combining the displacement decompositions given by Equations (34)–(36)

Given: material properties, $L_{ijmn}(\mathbf{y})$ and d is Dirac delta function.
Find: $\tilde{\Xi}_{ikl}(\mathbf{y}, \hat{\mathbf{y}}) : \overline{\mathcal{Y}} \times \overline{\mathcal{Y}} \to \mathbb{R}$ such that:

- Equilibrium:

$$\left\{ L_{ijmn}(\mathbf{y})\left(\tilde{\Xi}_{(m, y_n)kl}(\mathbf{y}, \hat{\mathbf{y}}) - \hat{z}I_{mnkl}d(\mathbf{y} - \hat{\mathbf{y}})\right)\right\}_{,y_j} = 0; \quad \mathbf{y}, \hat{\mathbf{y}} \in \mathcal{Y}$$

- Boundary conditions:
  - $\tilde{\Xi}_{ik\beta}$ periodic on $\mathbf{y} \in \Gamma_0^{\mathcal{Y}}$
  - $L_{ijmn}(\mathbf{y})\left(\tilde{\Xi}_{(m, y_n)kl}(\mathbf{y}, \hat{\mathbf{y}}) - \hat{z}I_{mnkl}d(\mathbf{y} - \hat{\mathbf{y}})\right)n_j = 0$ on $\mathbf{y} \in \Gamma_\pm^{\mathcal{Y}}$

Box 6: The second-order damage influence function problem (DIF^2).

with the $O(1)$ kinematic and constitutive expressions (Equations (25b) and (27)):

$$\sigma_{ij}^1(x, \mathbf{y}, t) = L_{ijkl}(\mathbf{y})A_{kl\alpha\beta}(\mathbf{y})u_{\alpha, x_\beta}(x, t) - L_{ijkl}(\mathbf{y})E_{kl\alpha\beta}(\mathbf{y})\omega_{, x_\alpha x_\beta}(x, t)$$
$$+ L_{ijkl}(\mathbf{y}) \int_{\mathcal{Y}} \tilde{A}_{klmn}(\mathbf{y}, \hat{\mathbf{y}})\overline{\mu}_{mn}(x, \hat{\mathbf{y}}, t)\mathrm{d}\hat{\mathbf{y}} \quad (38)$$
$$+ L_{ijkl}(\mathbf{y}) \int_{\mathcal{Y}} \tilde{E}_{klmn}(\mathbf{y}, \hat{\mathbf{y}})\hat{\mu}_{mn}(x, \hat{\mathbf{y}}, t)\mathrm{d}\hat{\mathbf{y}}$$

in which,

$$A_{ij\alpha\beta}(\mathbf{y}) = I_{ij\alpha\beta} + \Theta_{(i, y_j)\alpha\beta}(\mathbf{y});$$
$$E_{ij\alpha\beta}(\mathbf{y}) = I_{ij\alpha\beta} - \hat{z}\Xi_{(i, y_j)\alpha\beta}(\mathbf{y})$$
$$\tilde{A}_{ijkl}(\mathbf{y}, \hat{\mathbf{y}}) = \tilde{\Theta}_{(i, y_j)kl}(\mathbf{y}, \hat{\mathbf{y}}) - d(\hat{\mathbf{y}} - \mathbf{y})I_{ijkl}; \quad (39)$$
$$\tilde{E}_{ijkl}(\mathbf{y}, \hat{\mathbf{y}}) = \tilde{\Xi}_{(i, y_j)kl}(\mathbf{y}, \hat{\mathbf{y}}) - d(\hat{\mathbf{y}} - \mathbf{y})I_{ijkl}$$

Premultiplying the equilibrium equations for the influence function problems, EIF^1, EIF^2, DIF^1, and DIF^2 shown in Boxes 4, 5, 2, and 6, respectively, by $z\delta_{ip}$ ($p = 1, 2, 3$) and integrating over the RVE leads to:

$$A_{3j\alpha\beta}^{\mathcal{Y}} = 0; \quad E_{3j\alpha\beta}^{\mathcal{Y}} = 0$$
$$T_{3jkl}^{\mathcal{Y}} = 0; \quad H_{3jkl}^{\mathcal{Y}} = 0 \quad (40)$$

where the coefficient tensors $A_{ij\alpha\beta}^{\mathcal{Y}}$, $E_{ij\alpha\beta}^{\mathcal{Y}}$, $T_{ijkl}^{\mathcal{Y}}$ and $H_{ijkl}^{\mathcal{Y}}$ are defined as:

$$A_{ij\alpha\beta}^{\mathcal{Y}} = \left\langle L_{ijkl}(\mathbf{y})A_{kl\alpha\beta}(\mathbf{y})\right\rangle; \qquad E_{ij\alpha\beta}^{\mathcal{Y}} = \left\langle L_{ijkl}(\mathbf{y})E_{kl\alpha\beta}(\mathbf{y})\right\rangle$$

$$T_{ijkl}^{\mathcal{Y}} = \left\langle L_{ijmn}(\mathbf{y})\tilde{A}_{mnkl}(\mathbf{y},\hat{\mathbf{y}})\right\rangle; \qquad H_{ijkl}^{\mathcal{Y}}\left\langle L_{ijmn}(\mathbf{y})\tilde{E}_{mnkl}(\mathbf{y},\hat{\mathbf{y}})\right\rangle$$

(41)

Applying the averaging operator to Equation (38) and using Equations (41), Equation (37) is satisfied. The above argument is justified when $\delta_{ip}z$ is within the appropriate trial function space, which is automatically ensured for Equation (40a) when the EIF[1] and EIF[2] problems are evaluated within the classical finite element method framework. A numerical approximation of the DIF[1] and DIF[2] problems (described in Oskay and Fish, 2007) ensures the admissibility of $\delta_{ip}z$ for Equation (40b).

Macroscale Problem

We introduce the force, moment, and shear resultants based on the averaging of the stress components over the RVE:

$$\mathcal{N}_{\alpha\beta}(x,t) := \left\langle \sigma_{\alpha\beta}^1 \right\rangle; \quad \mathcal{M}_{\alpha\beta}(x,t) := \left\langle \hat{z}\sigma_{\alpha\beta}^1 \right\rangle; \quad \mathcal{Q}_\alpha(x,t) := \left\langle \sigma_{3\alpha}^2 \right\rangle \qquad (42)$$

Averaging the $O(\zeta)$ momentum balance equation (Equation (29c)) over the RVE, employing the $O(\zeta^2)$ boundary conditions, along with Equation (37):

$$\mathcal{N}_{\alpha\beta,x_\beta}(x,t) + q_\alpha(x,t) = \langle\rho\rangle\ddot{u}_\alpha(x,t) - \langle\rho\hat{z}\rangle\ddot{w}_{,x_\alpha}(x,t) \qquad (43)$$

where, q_α denotes the traction acting at the top and bottom surfaces of the plate as well as the body forces:

$$q_\alpha(x,t) = \langle b_\alpha\rangle(x,t) + \left\langle G_+\right\rangle_Y \bar{\tau}_\alpha^+(x,t) + \langle G_-\rangle_Y \bar{\tau}_\alpha^-(x,t) \qquad (44)$$

and $\langle\cdot\rangle_Y = \int_Y \cdot\, dy$, and;

$$G_\pm(y) = \sqrt{(1 + c_{,y_1}^\pm + c_{,y_2}^\pm)} \qquad (45)$$

accounts for the arbitrary shape of the RVE boundaries. Premultiplying Equation (29c) with $\hat{z}$ and averaging over the RVE yields:

$$\mathcal{M}_{\alpha\beta,x_\beta}(x,t) - \mathcal{Q}_\alpha(x,t) + p_\alpha(x,t) = \langle\rho\hat{z}\rangle\ddot{u}_\alpha(x,t) - \left\langle\rho\hat{z}^2\right\rangle\ddot{w}_{,x_\alpha}(x,t) \qquad (46)$$

where,

$$p_\alpha(x,t) = \langle \hat{z} b_\alpha \rangle(x,t) + \langle (c^+ - \langle z \rangle) G_+ \rangle_Y \overline{\tau}_\alpha^+(x,t) + \langle (c^- - \langle z \rangle) G_- \rangle_Y \overline{\tau}_\alpha^-(x,t) \quad (47)$$

Averaging the $O(\zeta^2)$ momentum balance equation (Equation (29d)) over the RVE, and using $O(\zeta^3)$ boundary condition yields:

$$\mathcal{Q}_{\alpha,x_\alpha}(x,t) + m(x,t) = \langle \rho \rangle \ddot{w}(x,t) \quad (48)$$

in which,

$$m(x,t) = \langle b_3 \rangle(x,t) + \langle G_+ \rangle_Y \overline{\tau}_3^+(x,t) + \langle G_- \rangle_Y \overline{\tau}_3^-(x,t) \quad (49)$$

The constitutive relationships for the force and moment resultants as a function of in-plane strains ($e_{\alpha\beta} = u_{\alpha,x_\beta}$) and curvature ($\kappa_{\alpha\beta} = -w_{,x_\alpha x_\beta}$), are obtained by averaging Equation (38) over the RVE:

$$\mathcal{N}_{\alpha\beta}(x,t) = A^{\mathcal{Y}}_{\alpha\beta\mu\eta} e_{\mu\eta}(x,t) + E^{\mathcal{Y}}_{\alpha\beta\mu\eta} \kappa_{\mu\eta}(x,t) +$$
$$\int_{\mathcal{Y}} T^{\mathcal{Y}}_{\alpha\beta kl}(\hat{\mathbf{y}}) \overline{\mu}_{kl}(x,\hat{\mathbf{y}},t) \mathrm{d}\hat{\mathbf{y}} + \int_{\mathcal{Y}} H^{\mathcal{Y}}_{\alpha\beta kl}(\hat{\mathbf{y}}) \hat{\mu}_{kl}(x,\hat{\mathbf{y}},t) \mathrm{d}\hat{\mathbf{y}} \quad (50)$$

$$\mathcal{M}_{\alpha\beta}(x,t) = F^{\mathcal{Y}}_{\alpha\beta\mu\eta} e_{\mu\eta}(x,t) + D^{\mathcal{Y}}_{\alpha\beta\mu\eta} \kappa_{\mu\eta}(x,t) +$$
$$\int_{\mathcal{Y}} G^{\mathcal{Y}}_{\alpha\beta kl}(\hat{\mathbf{y}}) \overline{\mu}_{kl}(x,\hat{\mathbf{y}},t) \mathrm{d}\hat{\mathbf{y}} + \int_{\mathcal{Y}} C^{\mathcal{Y}}_{\alpha\beta kl}(\hat{\mathbf{y}}) \hat{\mu}_{kl}(x,\hat{\mathbf{y}},t) \mathrm{d}\hat{\mathbf{y}} \quad (51)$$

where, the coefficient tensors, $F^{\mathcal{Y}}_{\alpha\beta\mu\eta}, D^{\mathcal{Y}}_{\alpha\beta\mu\eta}, G^{\mathcal{Y}}_{\alpha\beta kl}(\hat{\mathbf{y}})$, and $C^{\mathcal{Y}}_{\alpha\beta kl}(\hat{\mathbf{y}})$ are defined as:

$$F^{\mathcal{Y}}_{\alpha\beta\mu\eta} = \langle \hat{z} L_{\alpha\beta\gamma\xi}(\mathbf{y}) A_{\gamma\xi\mu\eta}(\mathbf{y}) \rangle; \qquad D^{\mathcal{Y}}_{\alpha\beta\mu\eta} = \langle \hat{z} L_{\alpha\beta\gamma\xi}(\mathbf{y}) E_{\gamma\xi\mu\eta}(\mathbf{y}) \rangle$$
$$G^{\mathcal{Y}}_{\alpha\beta kl}(\hat{\mathbf{y}}) = \langle \hat{z} L_{\alpha\beta ij}(\mathbf{y}) \tilde{A}_{ijkl}(\mathbf{y},\hat{\mathbf{y}}) \rangle; \quad C^{\mathcal{Y}}_{\alpha\beta kl}(\hat{\mathbf{y}}) = \langle \hat{z} L_{\alpha\beta ij}(\mathbf{y}) \tilde{E}_{ijkl}(\mathbf{y},\hat{\mathbf{y}}) \rangle \quad (52)$$

BOUNDARY CONDITIONS

To complete the formulation of the macroscopic problem, it remains to define the boundary conditions along Γ_0. Formulations of boundary conditions in the context of elastic beam and plate theories have been proposed in the past by a number of researchers based on decay analysis (Gregory and Wan, 1984; Buannic and Cartraud, 2001), inner expansions (Dauge et al., 2000), approximate conditions using integral forms (Timoshenko and Goodier, 1970), among others. While the former

two approaches are more rigorous and accurate, they are computationally expensive for nonlinear analysis due to the requirement of evaluation auxiliary problems to evaluate the solution close to the boundaries. In this manuscript, the original boundary conditions along Γ_0 are assumed to be of the following form:

$$u_i^\zeta(\mathbf{x}, t) = r^\zeta(\mathbf{x}, t); \quad \text{on } \Gamma_0^r \tag{53}$$

$$\sigma_{ij}^\zeta(\mathbf{x}, t)n_j = \tau_i^\zeta(\mathbf{x}, t); \quad \text{on } \Gamma_0^\tau \tag{54}$$

where, boundary partitions satisfy: $\Gamma_0 = \Gamma_0^r \cup \Gamma_0^\tau$, $\Gamma_0^r \cap \Gamma_0^\tau = \emptyset$. Along the displacement boundaries, Γ_0^r the displacement data of the following form is admitted

$$r^\zeta(\mathbf{x}, t) = \delta_{i3}W(x, t) + \zeta\delta_{i\alpha}[r_\alpha(x, t) - \hat{z}\theta_\alpha(x, t)] \tag{55}$$

Matching the displacement terms of zeroth and first orders along the boundary gives

$$O(1): \quad w(x, t) = W(x, t) \tag{56}$$

$$O(\zeta): \quad u_\alpha - \hat{z}w_{,x_\alpha} = r_\alpha(x, t) - \hat{z}\theta_\alpha(x, t) \tag{57}$$

Averaging Equation (57) over the RVE boundary gives the remaining displacement and rotation boundary conditions

$$u_\alpha = r_\alpha; \quad w_{,x_\alpha} = \theta_\alpha; \quad \text{on } \Gamma_0^r \tag{58}$$

Along the traction boundaries, Γ_0^τ, the traction data is assumed to satisfy the following scaling relations with respect to ζ

$$\tau_i^\zeta = \zeta\delta_{i\alpha}\tau_\alpha(x, t) + \zeta^2\delta_{i3}\tau_3(x, t) \tag{59}$$

The traction boundaries are satisfied approximately in the integral form. The equivalence relation between the average and exact boundary conditions may be shown based on the Saint Venant principle (Timoshenko and Goodier, 1970). The moment, force, and shear resultant boundary conditions are given as:

$$\mathcal{N}_{\alpha\beta}n_\beta = \tau_\alpha; \quad \mathcal{M}_{\alpha\beta}n_\beta = \langle\hat{z}\rangle\tau_\alpha; \quad \mathcal{Q}_\alpha n_\alpha = \tau_3 \tag{60}$$

Boundary data is taken to satisfy the free-edge condition (Reddy, 1997).

REDUCED-ORDER MODEL FOR THIN PLATES

The eigenstrain-based homogenization of the governing equations of a thin heterogeneous structure leads to a macroscopic problem with balance equations provided by Equations (43), (46), and (48) along with the constitutive relations (Equations (50) and (51)). The damage induced inelastic strain tensors $\overline{\mu}_{ij}$ and $\hat{\mu}_{ij}$ account for the coupling between the microscopic and macroscopic problems. We seek to solve the macroscopic problem in a computationally efficient manner. To this extent, the damage variable and eigenstrains are described as:

$$
\begin{Bmatrix} \overline{\mu}_{ij} \\ \hat{\mu}_{ij} \\ \omega \end{Bmatrix} (x, \mathbf{y}, t) = \sum_{I=1}^{n} \begin{Bmatrix} \overline{N}^{(I)}(\mathbf{y})\overline{\mu}_{ij}^{(I)}(x, t) \\ \hat{N}^{(I)}(\mathbf{y})\hat{\mu}_{ij}^{(I)}(x, t) \\ \vartheta^{(I)}(\mathbf{y})\omega^{(I)}(x, t) \end{Bmatrix}
\tag{61}
$$

where, $\overline{N}^{(I)}$, $\hat{N}^{(I)}$, and $\vartheta^{(I)}$ are shape functions, and; $\overline{\mu}_{ij}^{(I)}$, $\hat{\mu}_{ij}^{(I)}$, and $\omega^{(I)}(x, t)$ are the weighted average planar deformation, bending induced inelastic strain, and damage fields, respectively:

$$
\begin{Bmatrix} \overline{\mu}_{ij}^{(I)} \\ \hat{\mu}_{ij}^{(I)} \\ \omega^{(I)} \end{Bmatrix} (x, t) = \int_{\mathcal{Y}} \begin{Bmatrix} \overline{\psi}^{(I)}(\mathbf{y})\overline{\mu}_{ij}(x, \mathbf{y}, t) \\ \hat{\psi}^{(I)}(\mathbf{y})\hat{\mu}_{ij}(x, \mathbf{y}, t) \\ \eta^{(I)}(\mathbf{y})\omega(x, \mathbf{y}, t) \end{Bmatrix} d\mathbf{y}
\tag{62}
$$

where, $\overline{\psi}^{(I)}$, $\hat{\psi}^{(I)}$, and $\eta^{(I)}$ are microscopically nonlocal weight functions. The discretization of macroscopic and microscopic inelastic strains results in reduction in number of kinematic equations for the system, which in turn improves the computational efficiency of the model. The shape functions are taken to satisfy partition of unity property, while the weight are positive, normalized and orthonormal with respect to shape functions (Oskay and Fish, 2007):

$$
\sum_{I=1}^{n} N^{(I)}(\mathbf{y}) = 1; \quad \varphi^{(I)}(\mathbf{y}) \geq 0; \quad \int_{\mathcal{Y}} \varphi^{(I)}(\mathbf{y})d\mathbf{y} = 1;
$$
$$
\int_{\mathcal{Y}} \varphi^{(I)}(\mathbf{y})N^{(J)}(\mathbf{y})d\mathbf{y} = \delta_{IJ}
\tag{63}
$$

where $N^{(I)}$ and $\varphi^{(I)}$ denote any of the shape and weight functions, respectively. The in-plane deformation and bending induced inelastic strain fields may be expressed as:

$$\overline{\mu}_{ij}(x, \mathbf{y}, t) = \omega(x, \mathbf{y}, t)$$
$$\left(\delta_{i\alpha}\delta_{j\beta}e_{\alpha\beta}(x,t) + \frac{1}{2}\left(\delta_{i3}\delta_{j\alpha} + \delta_{i\alpha}\delta_{j3}\right)u_{3,x_\alpha}(x,t) + u^{2u}_{(i,y_j)}(x,\mathbf{y},t) \right) \quad (64)$$

$$\hat{\mu}_{ij}(x,\mathbf{y},t) = \omega(x,\mathbf{y},t)\left(\delta_{i\alpha}\delta_{j\beta}\hat{z}\kappa_{\alpha\beta}(x,t) + u^{2w}_{(i,y_j)}(x,\mathbf{y},t)\right) \quad (65)$$

Expressions for $\overline{\mu}^{(I)}_{ij}$ and $\hat{\mu}^{(I)}_{ij}$ are obtained by substituting Equations (35) and (36) into Equations (64) and (65), respectively and employing the inelastic field discretizations (Equations (61)–(63)):

$$\overline{\mu}^{(I)}_{ij}(x,t) = \omega^{(I)}(x,t)\left(A^{(I)}_{ij\mu\eta}e_{\mu\eta}(x,t) + \sum_J P^{(IJ)}_{ijkl}\overline{\mu}^{(J)}_{kl}(x,t)\right) \quad (66)$$

$$\hat{\mu}^{(I)}_{ij}(x,t) = \omega^{(I)}(x,t)\left(E^{(I)}_{ij\mu\eta}\kappa_{\mu\eta}(x,t) + \sum_J Q^{(IJ)}_{ijkl}\hat{\mu}^{(J)}_{kl}(x,t)\right) \quad (67)$$

in which, the coefficient tensors, $A^{(I)}_{ij\mu\eta}$, $E^{(I)}_{ij\mu\eta}$, $P^{(IJ)}_{ijkl}$, and $Q^{(IJ)}_{ijkl}$, are:

$$A^{(I)}_{ij\mu\eta} = \int_{\mathcal{Y}} \overline{\psi}^{(I)}(\mathbf{y})\vartheta^{(I)}(\mathbf{y})A_{ij\mu\eta}(\mathbf{y})d\mathbf{y}; \quad E^{(I)}_{ij\mu\eta} = \int_{\mathcal{Y}} \hat{\psi}^{(I)}(\mathbf{y})\vartheta^{(I)}(\mathbf{y})E_{ij\mu\eta}(\mathbf{y})d\mathbf{y} \quad (68)$$

$$P^{(IJ)}_{\alpha\beta\mu\eta} = \int_{\mathcal{Y}} \overline{\psi}^{(I)}(\mathbf{y})\vartheta^{(I)}(\mathbf{y})P^{(J)}_{\alpha\beta\mu\eta}(\mathbf{y})d\mathbf{y}; \quad Q^{(IJ)}_{\alpha\beta\mu\eta} = \int_{\mathcal{Y}} \hat{\psi}^{(I)}(\mathbf{y})\vartheta^{(I)}(\mathbf{y})Q^{(J)}_{\alpha\beta\mu\eta}(\mathbf{y})d\mathbf{y} \quad (69)$$

Employing the eigenstrain and damage decompositions, the in-plane force and moment resultants are expressed in terms of the phase average fields as

$$\mathcal{N}_{\alpha\beta}(x,t) = A^{\mathcal{Y}}_{\alpha\beta\mu\eta}e_{\mu\eta}(x,t) + E^{\mathcal{Y}}_{\alpha\beta\mu\eta}\kappa_{\mu\eta}(x,t)$$
$$+ \sum_{I=1}^{n}\left(T^{(I)}_{\alpha\beta kl}\overline{\mu}^{(I)}_{kl}(x,t) + H^{(I)}_{\alpha\beta kl}\hat{\mu}^{(I)}_{kl}(x,t)\right) \quad (70)$$

$$\mathcal{M}_{\alpha\beta}(x,t) = F^{\mathcal{Y}}_{\alpha\beta\mu\eta}e_{\mu\eta}(x,t) + D^{\mathcal{Y}}_{\alpha\beta\mu\eta}\kappa_{\mu\eta}(x,t)$$
$$+ \sum_{I=1}^{n}\left(G^{(I)}_{\alpha\beta kl}\overline{\mu}^{(I)}_{kl}(x,t) + C^{(I)}_{\alpha\beta kl}\hat{\mu}^{(I)}_{kl}(x,t)\right) \quad (71)$$

The coefficient tensors are expressed in terms of the damage influence functions:

$$P_{ijkl}^{(I)}(\mathbf{y}) = \int_{\mathcal{Y}} \overline{N}^{(I)}(\mathbf{y})\tilde{\Theta}_{(i,y_j)kl}(\mathbf{y})\mathrm{d}\mathbf{y}; \quad Q_{ijkl}^{(I)}(\mathbf{y}) = \int_{\mathcal{Y}} \hat{N}^{(I)}(\mathbf{y})\tilde{\Xi}_{(i,y_j)kl}(\mathbf{y})\mathrm{d}\mathbf{y} \quad (72)$$

$$T_{\alpha\beta kl}^{(I)} = \left\langle L_{\alpha\beta ij}\left[P_{ijkl}^{(I)}(\mathbf{y}) - I_{ijkl}\overline{N}^{(I)}(\mathbf{y})\right]\right\rangle;$$

$$H_{\alpha\beta kl}^{(I)} = \left\langle L_{\alpha\beta ij}\left[Q_{ijkl}^{(I)}(\mathbf{y}) - I_{ijkl}\hat{N}^{(I)}(\mathbf{y})\right]\right\rangle \quad (73)$$

$$G_{\alpha\beta kl}^{(I)} = \left\langle \hat{z}L_{\alpha\beta ij}\left[P_{ijkl}^{(I)}(\mathbf{y}) - I_{ijkl}\overline{N}^{(I)}(\mathbf{y})\right]\right\rangle;$$

$$C_{\alpha\beta kl}^{(I)} = \left\langle \hat{z}L_{\alpha\beta ij}\left[Q_{ijkl}^{(I)}(\mathbf{y}) - I_{ijkl}\hat{N}^{(I)}(\mathbf{y})\right]\right\rangle \quad (74)$$

The reduced-order macroscopic problem is summarized in Box 7.

Remark 4:

The verification studies provided below are conducted by choosing identical shape functions to define the inelastic field discretizations (i.e., $N^{(I)} = \overline{N}^{(I)} = \hat{N}^{(I)} = \vartheta^{(I)}$ and $\psi^{(I)} = \overline{\psi}^{(I)} = \hat{\psi}^{(I)} = \eta^{(I)}$) such that:

$$N^{(I)}(\mathbf{y}) = \begin{cases} 1 & \text{if } \mathbf{y} \in \mathcal{Y}^{(I)} \\ 0 & \text{elsewhere} \end{cases}$$

$$\psi^{(I)}(\mathbf{y}) = \frac{1}{|\mathcal{Y}^{(I)}|} N^{(I)}(\mathbf{y})$$

where, $\mathcal{Y}^{(I)}$ is the Ith partition in $\mathcal{Y}$. The partitions are disjoint subdomains filling the entire microstructure (i.e., $\mathcal{Y} \equiv \bigcup_{I=1}^{n} \mathcal{Y}^{(I)}$ and $\mathcal{Y}^{(I)} \bigcap \mathcal{Y}^{(J)} \equiv \emptyset$ for $I \neq J$) and each subdomain resides in a single physical phase. $N^{(I)}$ and $\psi^{(I)}$ are the simplest functions that satisfy partition of unity, positivity, normality and orthonormality conditions given in Equation (63).

Rate-dependent Damage Evolution Model

The inelastic processes within the microstructure is idealized using the damage variables, $\omega^{(I)}$. In this manuscript a rate-dependent model is used to characterize the evolution of damage within the microstructure (Simo and Ju, 1987):

A potential damage function, f, is defined:

$$f(\upsilon^{(I)}, r^{(I)}) = \phi(\upsilon^{(I)}) - \phi(r^{(I)}) \leqslant 0 \quad (75)$$

Given: Influence functions, $\Theta_{i\alpha\beta}$, $\Xi_{i\alpha\beta}$, $\tilde{\Theta}_{ikl}$, $\tilde{\Xi}_{ikl}$, $L_{\alpha\beta kl}$, and; material parameters associated with the evolution of damage; boundary data r_α, θ_α, τ_α, $\tau_i^\pm$; body force, b_i; density, ρ, initial condition data, $\hat{w}$, $\overline{w}$, $\hat{u}_\alpha$, and $\hat{v}_\alpha$.

Find: macroscopic displacements u_α and $w_{,x_\alpha}$ such that:

- Momentum balance:

$$\mathcal{N}_{\alpha\beta,x_\beta}(x,t) + q_\alpha(x,t) = \langle\rho\rangle\ddot{u}_\alpha(x,t) - \langle\rho\hat{z}\rangle\ddot{w}_{,x_\alpha}(x,t)$$

$$\mathcal{M}_{\alpha\beta,x_\beta}(x,t) - \mathcal{Q}_\alpha(x,t) + p_\alpha(x,t) = \langle\rho\hat{z}\rangle\ddot{u}_\alpha(x,t) - \langle\rho\hat{z}^2\rangle\ddot{w}_{,x_\alpha}(x,t)$$

$$\mathcal{Q}_{\alpha,x_\alpha}(x,t) + m(x,t) = \langle\rho\rangle\ddot{w}(x,t)$$

- Constitutive relations:

$$\mathcal{N}_{\alpha\beta} = A^{\mathcal{Y}}_{\alpha\beta\mu\eta}e_{\mu\eta}(x,t) + E^{\mathcal{Y}}_{\alpha\beta\mu\eta}\kappa_{\mu\eta}(x,t) + \sum_{I=1}^{n}\left(T^{(I)}_{\alpha\beta kl}\overline{\mu}^{(I)}_{kl}(x,t) + H^{(I)}_{\alpha\beta kl}\hat{\mu}^{(I)}_{kl}(x,t)\right)$$

$$\mathcal{M}_{\alpha\beta} = F^{\mathcal{Y}}_{\alpha\beta\mu\eta}e_{\mu\eta}(x,t) + D^{\mathcal{Y}}_{\alpha\beta\mu\eta}\kappa_{\mu\eta}(x,t) + \sum_{I=1}^{n}\left(G^{(I)}_{\alpha\beta kl}\overline{\mu}^{(I)}_{kl}(x,t) + C^{(I)}_{\alpha\beta kl}\hat{\mu}^{(I)}_{kl}(x,t)\right)$$

$$\overline{\mu}^{(I)}_{\alpha\beta} = \omega^{(I)}(x,t)\left[A^{(I)}_{\alpha\beta\mu\eta}e_{\mu\eta}(x,t) + \sum_{J=1}^{n}P^{(IJ)}_{\alpha\beta\mu\eta}\overline{\mu}^{(J)}_{\mu\eta}(x,t)\right]$$

$$\hat{\mu}^{(I)}_{\alpha\beta} = \omega^{(I)}(x,t)\left[E^{(I)}_{\alpha\beta\mu\eta}e_{\mu\eta}(x,t) + \sum_{J=1}^{n}Q^{(IJ)}_{\alpha\beta\mu\eta}\hat{\mu}^{(J)}_{\mu\eta}(x,t)\right]$$

- Kinematics:

$$e_{\alpha\beta}(x,t) = u_{(\alpha,y_\beta)}(x,t); \quad \kappa_{\alpha\beta}(x,t) = -w_{,x_\alpha x_\beta}(x,t)$$

- Initial conditions ($x \in \Omega$):

$$w(x,t=0) = \hat{w}(x); \quad u_\alpha(x,t=0) = \hat{u}_\alpha(x)$$

$$\dot{w}(x,t=0) = \overline{w}(x); \quad \dot{u}_\alpha(x,t=0) = \hat{v}_\alpha(x)$$

- Boundary conditions:

$$u_\alpha = r_\alpha; \quad w_{,x_\alpha} = \theta_\alpha \quad \text{on } \Gamma_0^r$$

$$\mathcal{N}_{\alpha\beta}n_\beta = \langle\tau_\alpha\rangle; \quad \mathcal{M}_{\alpha\beta}n_\beta = \langle\hat{z}\tau_\alpha\rangle; \quad \mathcal{Q}_\alpha n_\alpha = \tau_3 \quad \text{on} \quad \Gamma_0^\tau$$

- Evolution equations for $\omega^{(I)}(x,\mathbf{y},t)$

Box 7: The reduced-order macroscopic problem (*n*-point model).

in which, $\upsilon^{(I)}(x, t)$, and $r^{(I)}(x, t)$ are phase damage equivalent strain and damage hardening variable, respectively, and; ϕ is a monotonically increasing damage evolution function. The evolution equations for $\upsilon^{(I)}$ and $r^{(I)}$ are given as

$$\dot{\omega}^{(I)} = \dot{\lambda} \frac{\partial \phi}{\partial \upsilon^{(I)}} \tag{76}$$

$$\dot{r}^{(I)} = \dot{\lambda} \tag{77}$$

where the evolution is based on a power law expression of the form:

$$\dot{\lambda} = \frac{1}{q^{(I)}} \langle f(\upsilon^{(I)}, r^{(I)}) \rangle_+^{p^{(I)}} \tag{78}$$

$\langle \cdot \rangle_+ = [\| \cdot | + (\cdot)]/2$ denotes MacCauley brackets; $p^{(I)}$ and $q^{(I)}$ define the rate-dependent response of damage evolution.

The phase damage equivalent strain is defined as

$$\upsilon^{(I)} = \sqrt{\frac{1}{2} \left(\mathbf{F}^{(I)} \hat{\epsilon}^{(I)}\right)^{\mathrm{T}} \hat{\mathbf{L}}^{(I)} \left(\mathbf{F}^{(I)} \hat{\epsilon}^{(I)}\right)} \tag{79}$$

in which, $\hat{\epsilon}^{(\eta)}$ is the average principal strain tensor in $\mathcal{Y}^{(I)}$; $\hat{\mathbf{L}}^{(I)}$ is the tensor of elastic moduli rotated onto the principal strain directions, and; $\mathbf{F}^{(I)}(\mathbf{x}, t)$ is the weighting matrix. The weighting matrix accounts for the anisotropic damage accumulation in tensile and compressive directions:

$$\mathbf{F}^{(\eta)} = \begin{bmatrix} h_1^{(I)} & 0 & 0 \\ 0 & h_2^{(I)} & 0 \\ 0 & 0 & h_3^{(I)} \end{bmatrix} \tag{80}$$

$$h_\xi^{(I)} = \frac{1}{2} + \frac{1}{\pi} \mathrm{atan}\left[c_1^{(I)}\left(\hat{\epsilon}_\xi^{(I)} - c_2^{(I)}\right)\right] \tag{81}$$

where, material parameters, $c_1^{(I)}$ and $c_2^{(I)}$, control damage accumulation in the tensile and compressive loading. A power law-based damage evolution function is considered:

$$\phi^{(I)}(\upsilon^{(I)}) = a^{(I)} \left\langle \upsilon^{(I)} - \upsilon_0^{(I)} \right\rangle_+^{b^{(I)}}; \quad \phi^{(I)} \leq 1 \tag{82}$$

in which, $a^{(I)}$ and $b^{(I)}$ are material parameters. The analytical form of $\phi^{(I)}(r^{(I)})$ is obtained by replacing $\upsilon^{(I)}$ by $r^{(I)}$ in Equation (82).

COMPUTATIONAL ASPECTS

The proposed multiscale model is implemented and incorporated into a commercial finite element analysis program (Abaqus). The implementation is a two stage process as illustrated in Figure 2. The first stage (pre-processing) consists of the evaluation of first and second-order RVE problems, summarized in Boxes 1 and 3, and computation of coefficient tensors. The preprocessing stage is evaluated using an in-house code, in which the linear elastic RVE problems are evaluated using the FEM. The model order, n, is taken to be a user defined input variable. By this approach, the coefficient tensors remain constant throughout the macroscale analysis. Alternative strategies are also possible, where the model order is updated based on the model error and accuracy (Oskay and Fish, 2007). A commercial finite element software (Abaqus) is employed to evaluate the macroscopic boundary value problem summarized in Box 7. User-defined generalized shell section behavior subroutine (UGENS) is implemented and incorporated into Abaqus to update force and moment resultants. The UGENS subroutine consists of computation of force ($\mathcal{N}$) and moment ($\mathcal{M}$) resultant at the current time step, given the generalized macroscale strain tensors (e, κ) and the damage state variable, $\omega^{(I)}$ at the previous time step and the generalized strain increments. Details of the procedure to evaluate the constitutive response in UGENS are lengthy yet straight forward. The procedure for constitutive update based on reduced-order damage models are provided in Oskay and Fish (2007). The Abaqus general purpose elements, S4R, are employed in the verification simulations.

Classical rate independent damage models are known to exhibit spurious mesh sensitivity when loading extends to the softening regime. This phenomenon is characterized by the localization of strains to within the
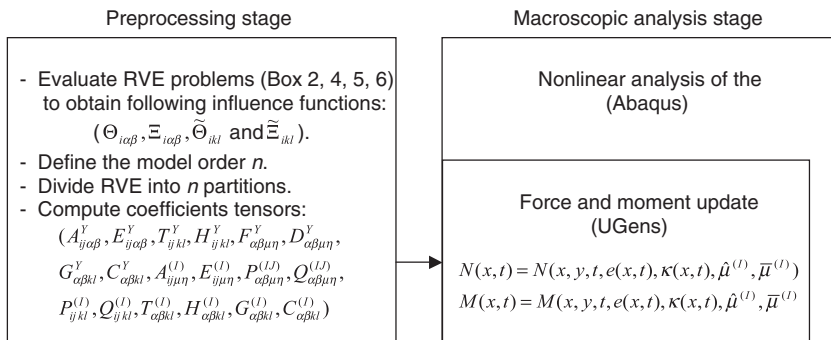
Preprocessing stage   Macroscopic analysis stage

- Evaluate RVE problems (Box 2, 4, 5, 6) to obtain following influence functions:

$$(\Theta_{i\alpha\beta}, \Xi_{i\alpha\beta}, \widetilde{\Theta}_{ikl} \text{ and } \widetilde{\Xi}_{ikl}).$$

- Define the model order n.
- Divide RVE into n partitions.
- Compute coefficients tensors:

$$(A^Y_{ij\alpha\beta}, E^Y_{ij\alpha\beta}, T^Y_{ijkl}, H^Y_{ijkl}, F^Y_{\alpha\beta\mu\eta}, D^Y_{\alpha\beta\mu\eta},$$
$$G^Y_{\alpha\beta kl}, C^Y_{\alpha\beta kl}, A^{(I)}_{ij\mu\eta}, E^{(I)}_{ij\mu\eta}, P^{(IJ)}_{\alpha\beta\mu\eta}, Q^{(IJ)}_{\alpha\beta\mu\eta},$$
$$P^{(I)}_{ijkl}, Q^{(I)}_{ijkl}, T^{(I)}_{\alpha\beta kl}, H^{(I)}_{\alpha\beta kl}, G^{(I)}_{\alpha\beta kl}, C^{(I)}_{\alpha\beta kl})$$

Nonlinear analysis of the (Abaqus)

Force and moment update (UGens)

$$N(x,t) = N(x, y, t, e(x,t), \kappa(x,t), \hat{\mu}^{(I)}, \overline{\mu}^{(I)})$$
$$M(x,t) = M(x, y, t, e(x,t), \kappa(x,t), \hat{\mu}^{(I)}, \overline{\mu}^{(I)}$$

Figure 2. *Implementation of the proposed multiscale model using the commercial finite element code Abaqus.*

size of a finite element. This problem is typically alleviated by considering gradient enhancement (de Borst and Muhlhaus, 1992; Al-Rub and Voyiadjis, 2006), nonlocal regularization of the integral type (Bazant et al., 1984), Cosserat continuum model (de Borst and Sluys, 1991) and viscous regularization (Needleman, 1988). Multiscale failure models based on damage mechanics may show mesh sensitivity at all associated scales. The proposed multiscale model is microscopically nonlocal through the integral-type nonlocal formulation presented in 'Reduced-order Model for Thin Plates' section. At the macroscopic scales, mesh sensitivity is alleviated by considering the viscous regularization of the damage model (Needleman, 1988). Viscous regularization permits the implementation within the standard finite element framework.

NUMERICAL VERIFICATION AND VALIDATION

The capabilities of the proposed multiscale plate model are assessed by considering three test cases: (a) three-point bending; (b) uniaxial tension, and (c) impact of rigid projectile on a woven composite plate. The model simulations are compared to direct 3D (reference) finite element models in which the microstructure is resolved throughout the macrostructure.

Three-point Plate Bending

We consider a three-point bending of a simply supported composite plate as shown in Figure 3. The dimensions of the rectangular plate are $W/L = 3/40$ and $t/L = 1/80$, in which t, W, and L are the thickness, width, and length of the plate, respectively. The small scaling parameter ζ can be calculated as the ratio between the thickness (or in-plane periodicity dimension) and the span length between the supports ($\epsilon = \zeta = 1/40$). A static vertical load is applied at the center of the plate quasi-statically until failure.

The microstructure consists of a matrix material reinforced with stiff unidirectional fibers oriented in the global z-direction as illustrated in Figure 3. The fiber fraction is 19% by volume. The stiffness contrast between the matrix and reinforcement phases is chosen to be $E^M/E^F = 0.3$, where, E^M and E^F are the Young's Modulus of the matrix and fiber, respectively. The Poisson's ratio of both materials is assumed to be identical ($v^F = v^M$). Damage evolution parameters are chosen to assure a linear dependence between the damage equivalent strain and evolution law (i.e., in Equation (82), $b^{(I)} = 1$). Damage is allowed to accumulate in tension only and no significant damage accumulation occurs under compressive loads. The fiber phase is assumed to be damage-free for the considered load amplitudes, and damage is allowed to accumulate in the matrix phase only.

The model parameters for the matrix and the fiber material are summarized in Table 1. The superscripts M and F denotes matrix and fiber phases respectively.

A suite of multiscale model simulations are conducted to verify the proposed approach. 3-, 5-, 13-, and 25-partition models are compared with 3D reference simulations. The microstructural partitions for the four multiscale models are illustrated in Figure 4. Simulations are conducted at three different load rates. An order of magnitude difference in the load rates are applied between the slow, intermediate, and fast simulations. Figure 5 illustrates the normalized force–displacement curves at the midspan of the plate. A reasonably good agreement is observed between the proposed multiscale models and reference simulations. The modeling error for the proposed models is tabulated in Table 2 for each multiscale model at each strain rate. It can be observed that while higher partition schemes tend to achieve better accuracy compared to lower partitions, a clear diminishing of error with increasing number of partitions does not occur. This is due to the nonoptimal selection
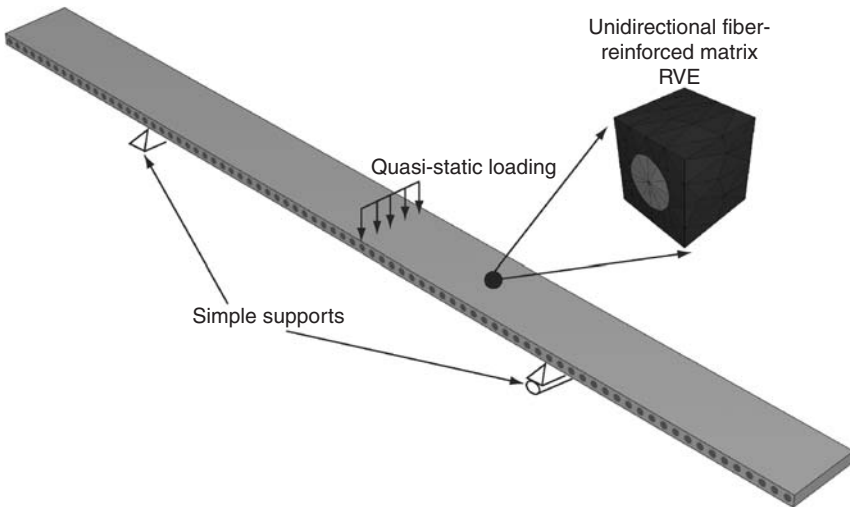
Figure 3. *Macro- and microscopic configurations of the three-point bending plate problem.*

Table 1. Material property values used in three-point bending and uniaxial tension test simulations.

$E^{(F)}$	$v^{(F)}$	$E^{(M)}$	$v^{(M)}$			
200 GPa	0.3	60 GPa	0.3			
$a^{(M)}$	$b^{(M)}$	$c_1^{(M)}$	$c_2^{(M)}$	$\upsilon_0^{(M)}$	$p^{(M)}$	$q^{(M)}$
0.75	1.0	1.e5	0.0	0.0	2.0	2.1

Table 2. Errors in terms of failure displacement, failure force, and L^2 norm in the force–displacement space.

Model	% error in failure displacement			% error in failure force			% L^2 error		
	Slow	Int.	Fast	Slow	Int.	Fast	Slow	Int.	Fast
$n = 3$	2.8189	2.0079	5.4234	0.6942	2.8026	3.9114	0.0295	0.0878	0.1520
$n = 5$	2.1551	0.69527	0.32336	3.082	0.47734	0.0471	0.0642	0.0488	0.0457
$n = 13$	5.0153	2.8458	4.8786	5.7351	2.9361	2.4879	0.1095	0.0740	0.0622
$n = 25$	0.1385	1.2027	0.9786	2.7725	1.0971	0.9417	0.0921	0.0660	0.0540
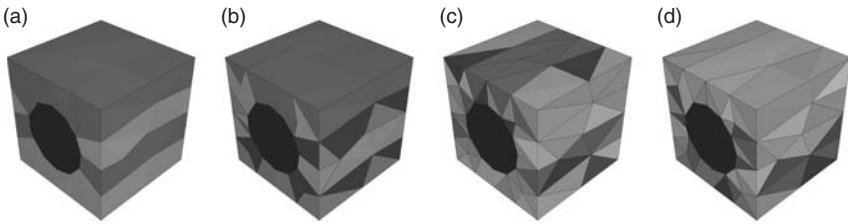
Figure 4. *Microstructural partitioning for (a) 3-partition, (b) 5-partition, (c) 13-partition, and (d) 25-partition models. Each partition is identified using separate colors.*
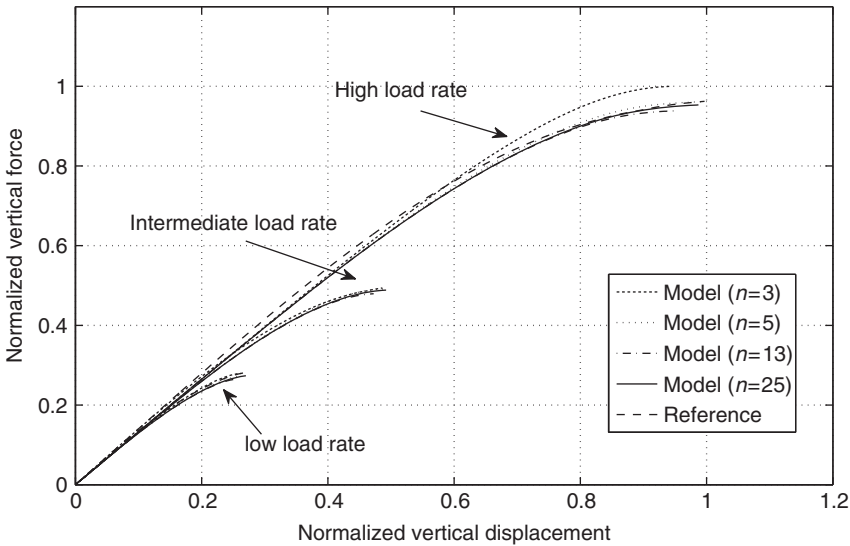
Figure 5. *Normalized force–displacement curves in three-point bending simulations. Multiscale simulation predictions compared to those of 3D reference simulations.*

of the domains of each partition, which significantly affects the quality of the model. The issue of optimal selection of partition domains is further discussed in 'Conclusions and Future Work' section. Displacement profiles at failure illustrated in Figure 6 also indicate similar trends observed above. The maximum error is observed in the 3-partition model simulations. Maximum normalized error occurs at the midspan of the plate (=6.5–9%). Damage contours at each partition of the 5-partition model is compared to the 3D reference simulations in Figure 7. The maximum damage is accumulated at the lowermost layer subjected to tensile loads. Upper layers are subjected to neutral and compressive loads leading to minimal damage accumulation. The 3D reference analysis plots indicate that failure starts at the bottom of the plate, which is subjected to higher tensile stresses.
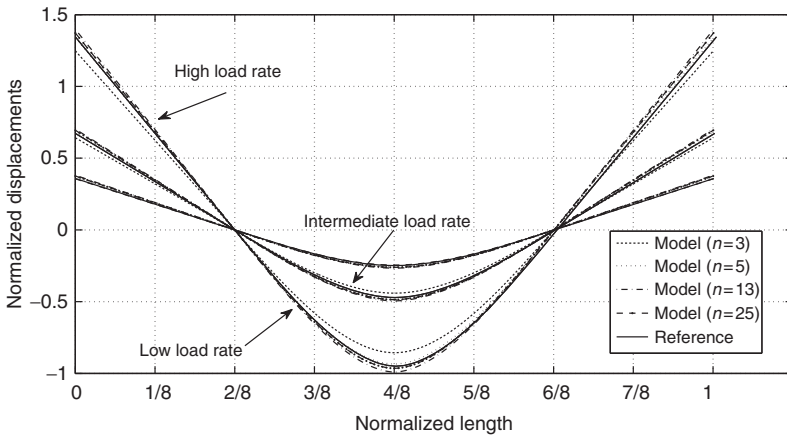
Figure 6. *Comparison of the displacements along the length of the plate, between the proposed multiscale models and 3D reference problem.*
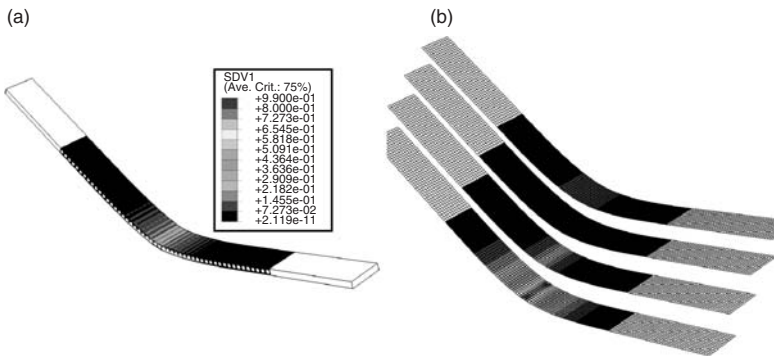
Figure 7. *Damage profile for (a) 3D reference simulation and (b) 5-partition model. Damage variables plotted correspond to damage in each matrix partition in the 5-partition model.*

Uniaxial Tension Test

We illustrate the nonlocal characteristics of the proposed multiscale model using a uniaxially loaded thin rectangular plate. The dimensions of the plate are $W/L = 1/5$ and $t/L = 1/30$. Two notches with half the thickness of the plate is placed at opposite edges of the plate 45^0 apart. Prescribed displacements are applied along the in-plane dimension parallel to the long edge. The microstructural configuration and material properties are identical to the three-point bending case discussed in the previous section. The model parameters for the matrix and the fiber material are summarized in Table 1.

A series of numerical simulations are conducted on three different finite element meshes with h/L ratios of $1/60$, $1/120$, and $1/240$ as shown in Figure 8. Two cases of microstructural orientation is considered: fibers are placed parallel and perpendicular to the stretch direction. Simulations are conducted using a 5-partition model ($n = 5$). Figure 9 illustrates the normalized force–displacement curves for coarse, intermediate, and fine meshes. The softening regime of the curves for both microstructural
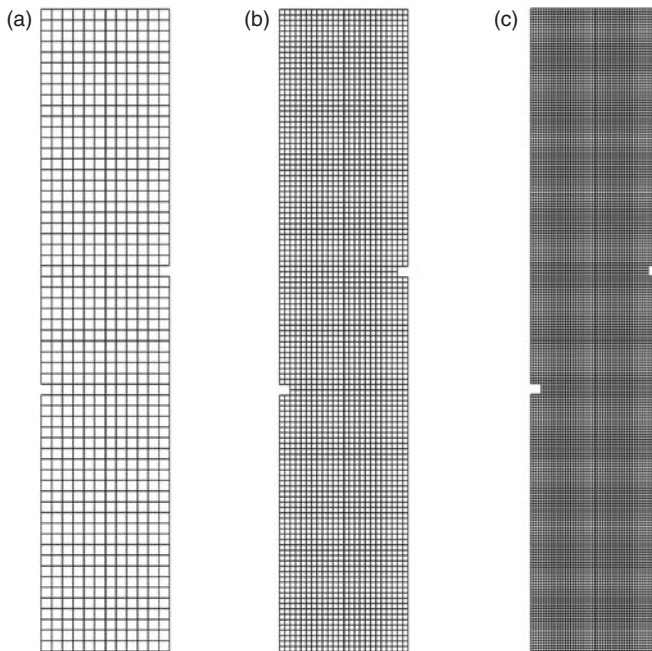
Figure 8. *Finite element discretization of the macroscopic plates: (a) coarse mesh (h/L = 1/60), (b) intermediate mesh (h/L = 1/120), and (c) fine mesh (h/L = 1/240).*

orientations shows nearly identical response for all three meshes, clearly indicating the mesh independent characteristic of the proposed multiscale model. In case of fibers parallel to the loading direction a 166% and 140% increase have been observed in the failure load and displacements, respectively. Figure 10 illustrates the damage fields ahead of the notches for the intermediate and fine meshes when the fibers are placed perpendicular to the loading direction. The contours correspond to the damage state at 75% of the failure displacement. The damage accumulation is observed to be along the direction of the elastic fibers.

High Velocity Impact Response of Woven Composite Plate

The capabilities of the proposed multiscale model are further verified by predicting the impact response of a composite plate. A 5-layer E-glass/polyester plain weave laminated composite system was experimentally investigated by Garcia-Castillo et al. (2006). The microstructure of the composite laminated plate is illustrated in Figure 11. The composite specimens are 140 mm × 200 mm rectangular plates with 3.19 mm thickness. The specimens were subjected to impact by steel projectiles with velocities ranging between 140 and 525 m/s. We employ the proposed multiscale model to predict the impact response of plates observed in the experiments.
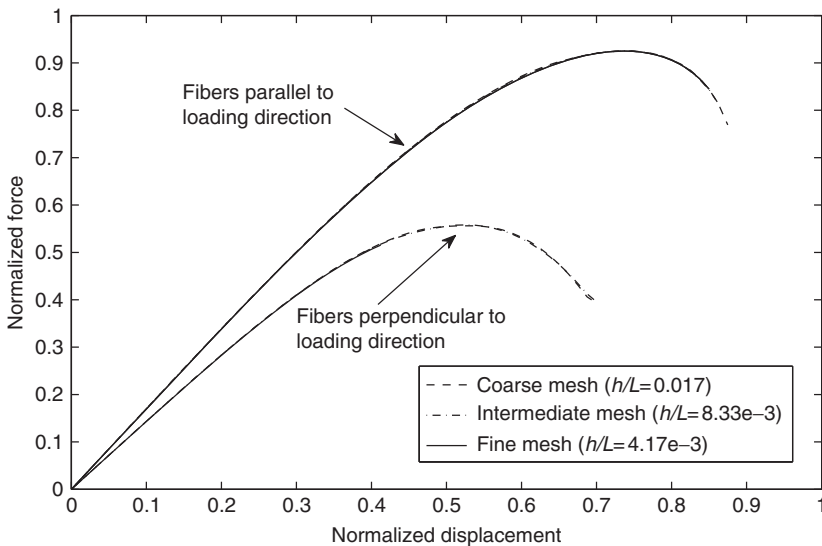

Figure 9. *Normalized force–displacement curves simulated using coarse, intermediate, and fine meshes for cases where fibers are placed parallel and perpendicular to the loading direction.*
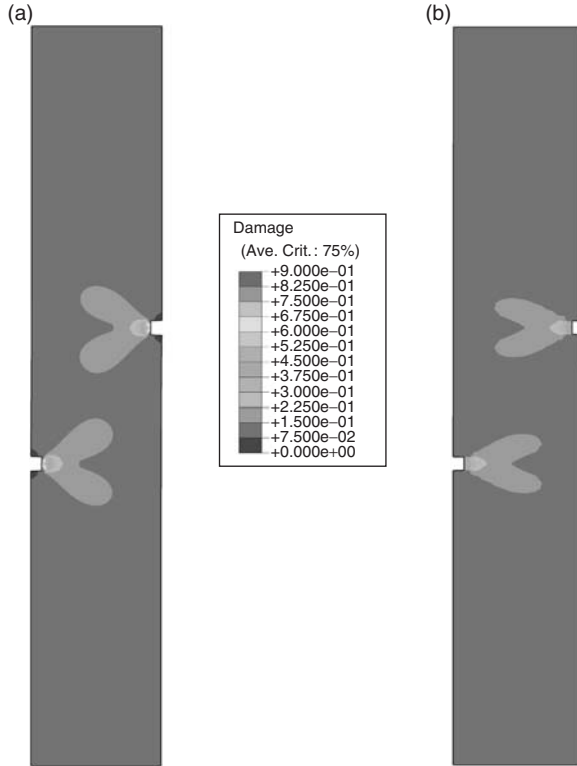
Figure 10. *Damage contour plots for (a) fine mesh and (b) intermediate mesh.*

A 19-partition model is employed. The plate consists of 5- plain weave plies with 0.276 mm thickness. A 34.5 µm thick ply-interphase layer is assumed to exist between each pair of plies in this 5-ply composite. The weave tows are in 0- and 90-directions. The fiber volume fractions are 9% in 0-direction and 22% in the 90-direction with a total of 31%. The matrix, fiber tows in 0- and 90-directions and ply-interphase in each layer is represented by a single partition totaling 19 for 5 plies.

Failure in each partition is modeled using the rate-dependent damage model described in 'Rate-dependent Damage Evolution Model' section. Material properties of fiber tows in 0- and 90-directions are taken to be identical. The ply-interphase and matrix properties are also assumed to be identical. The static response of the composite system when subjected to uniaxial tension is used to calibrate $a^{(I)}$ and $b^{(I)}$ parameters for matrix and reinforcement by minimizing the discrepancy between the reported
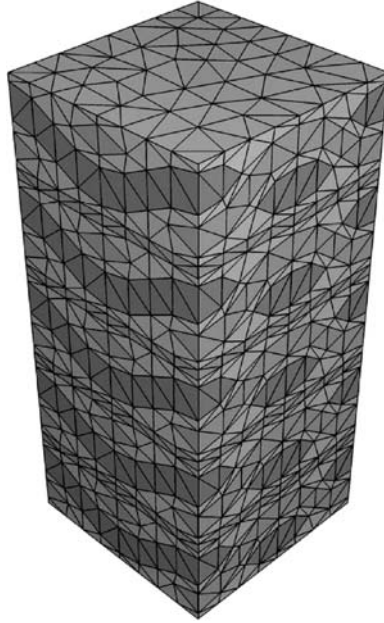
Figure 11. *Microstructure of the 5-ply woven laminate system.*

experimental failure stress and strain (3.6% and 367 MPa) and the simulated values (Figure 12). Genetic and gradient-based optimization algorithms are employed to calibrate the model parameters (Oskay and Fish, 2008). The stress–strain curves based on uniaxial tension as well as damage evolution in each microconstituent are shown in Figure 12 for loading in two orthogonal directions. The damage evolution parameter $a^{(I)}$ and $b^{(I)}$ were determined as 0.08 and 1.5 for fiber, and 0.92 and 2.5 for matrix materials, respectively. The fibers in 0 and 90, as well as the matrix and ply-interphase materials are assumed to have identical failure characteristics. A linear rate dependence is adopted for all microconstituents (i.e., $p^{(I)} = 1$). Damage is assumed to accumulate on the onset of loading ($v_0^{(I)} = 0$). Ply-interphase failure between all plies are observed in numerical simulations as indicated in Figure 12, which is in agreement with the experimentally observed response (Garcia-Castillo et al., 2006). Figure 11(a) and (b) illustrates the failure modes modeled in the simulations: Failure of the interphase between laminates, cracking within the matrix and fibers in the longitudinal and transverse directions. The effects of the fiber–matrix interface cracking is implicitly taken into account through the microconstituents cracking only. The failure of the interphase and the longitudinal fiber cracking (at 5% strain) precede
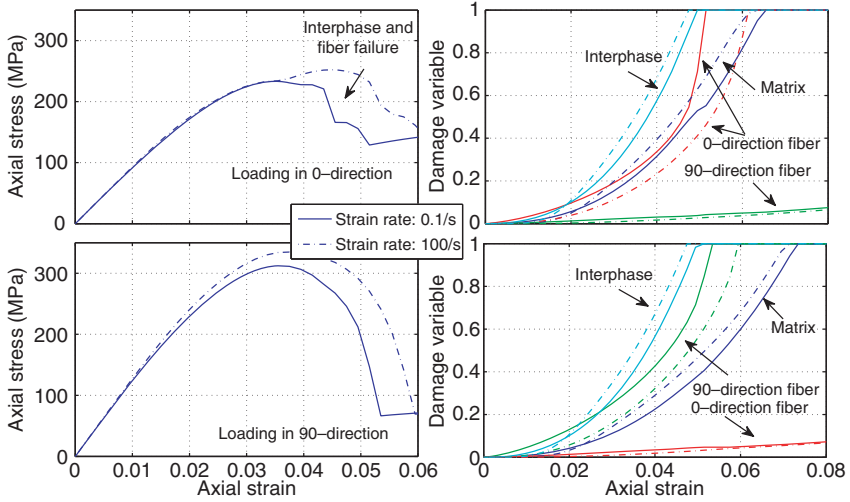
Figure 12. Simulations conducted under uniaxial tension: (a) stress–strain curves when subjected to 0.1/s and 100/s strain rates in the 0-direction; (b) damage evolution in interphase, matrix, and fiber phases for loading in the 0-direction; (c) stress–strain curves when subjected to 0.1/s and 100/s strain rates in the 90-direction; (d) damage evolution in interphase, matrix, and fiber phases for loading in the 90-direction.

the matrix cracking (at 7% strain). The damage in the transverse fiber cracking remains low throughout the uniaxial loading. The observations stated here remain to be verified by experimental observations since the authors did not have access to the tested specimen.

The exit velocities of the projectile when the composite specimen is subjected to impact velocities above the ballistic limit are predicted using the multiscale model. The experimentally provided ballistic limit value of 211 m/s is employed to calibrate the rate-dependent material parameter of the microconstituent failure models ($q^{(I)} = 1.8e-5$). Figure 13 shows the exit velocity of the projectile as a function of the impact velocity. The simulated response shows a nonlinear relationship in impact velocities close to the ballistic limit followed by a linearizing trend – similar to the experimental observations. The discrepancy between the experimental observations and the simulated exit velocities are attributed to the limited data used in the calibration of the microconstituent material parameters. Figure 14 provides ply-interphase damage regions for impact velocities of 211, 300, 400, and 500 m/s. The size of the ply-interphase damage region is observed to have only a slight variation with respect to the impact velocity, which is in agreement with the experimental response.
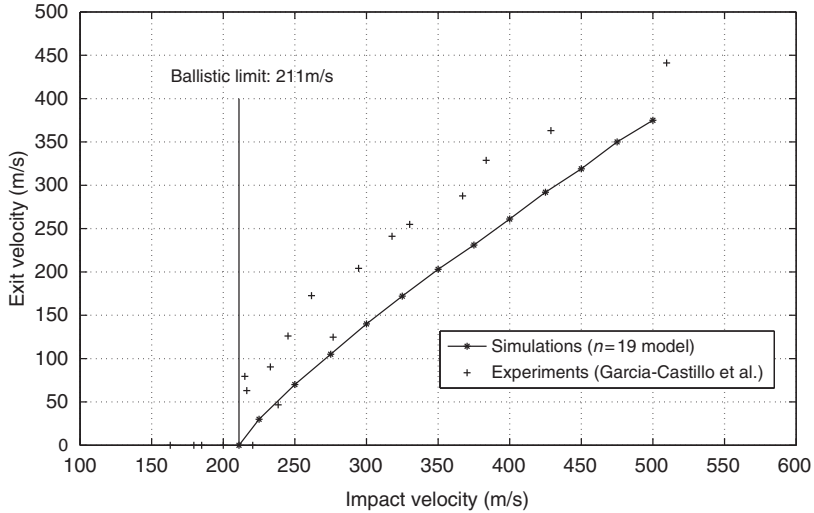
Figure 13. *Variation of the exit velocity with respect to impact velocity.*

CONCLUSIONS AND FUTURE WORK

We presented a new failure modeling approach for static and dynamic analysis of thin heterogeneous structures. The proposed approach is computationally advantageous compared to direct nonlinear computational homogenization technique in two respects: (1) the necessity of evaluating nonlinear microscopic boundary value problems at all integration points in the macroscopic finite element mesh is eliminated using the eigendeformation concept, and; (2) necessity to resolve the thickness direction in the macroscopic scale is alleviated by considering a structural theory based approach. A number of challenges remain. First is the thin plate assumptions present on the macroscopic displacement fields. It is well known that this restriction is prohibitive for thick plates and restricts the representable failure modes. A higher order displacement field – perhaps extending beyond first order or even layerwise theories – needs to be chosen to represent the macroscopic response without significantly compromising on the efficiency of the model. The second concern is the extension of the proposed approach to large microscopic strains. While our current approach is efficient for small deformations, generalization to large deformations is not clear within the framework of eigendeformation theory. The third issue concerns the proper selection of the microscopic partitions. The error analysis results indicate that the accuracy of the proposed multiscale model
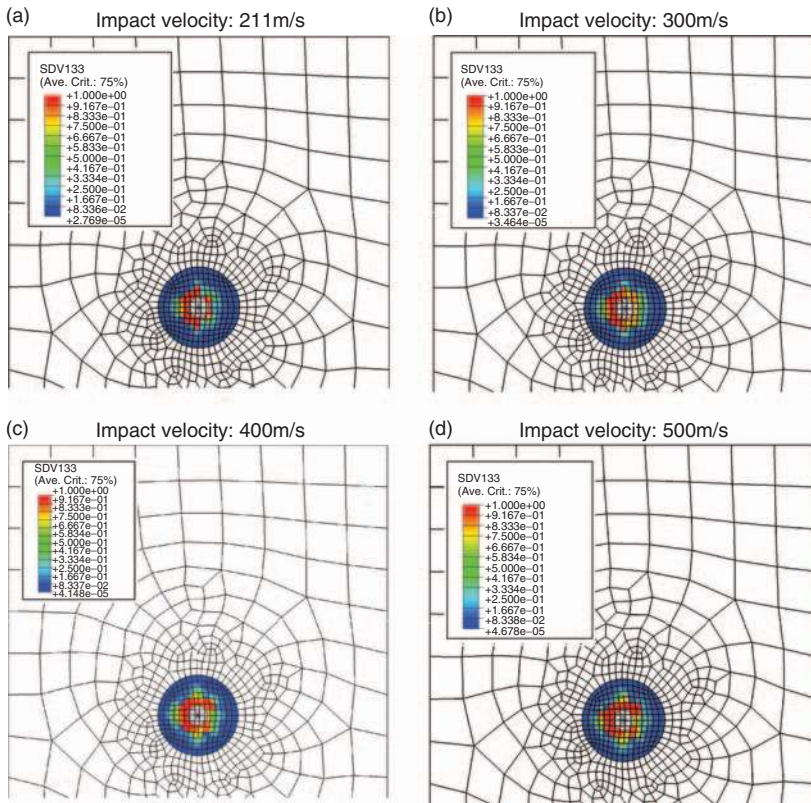
Figure 14. *Interphase damage variation around the impact zone at impact velocities (a) 211 m/s, (b) 300 m/s, (c) 400 m/s, (d) 500 m/s.*

is affected by the selection of the domain of each partition. Development of a robust partitioning strategy is therefore crucial in the minimization of the modeling errors. A final point is regarding the lack of consistent fragmentation criteria for heterogeneous materials. A detailed investigation of fragmentation is essential to correctly model the failure and fragmentation response of composite systems when subjected to penetration, crushing and blast problems. The issues outlined above require further investigation and will be explored by the authors.

ACKNOWLEDGMENT

REFERENCES

Al-Rub, A. and Voyiadjis, G.Z. (2006). A Finite Strain Plastic-damage Model for High Velocity Impact using Combined Viscosity and Gradient Localization Limiters: Part I – Theoretical Formulation, *Int. J. Damage Mech.*, **15**(4): 293–334.

Babuska, I. (1975). Homogenization and Application. Mathematical and Computational Problems, In: Hubbard, B. (ed.), *Numerical Solution of Partial Diferential Equations – III, SYNSPADE*, Academic press, College Park, MD, pp. 89–116.

Bahei-El-Din, Y.A., Rajendran, A.M. and Zikry, M.A. (2004). A Micromechanical Model for Damage Progression in Woven Composite Systems, *Int. J. Solid Struct.*, **41**(9–10): 2307–2330.

Baucom, J.N. and Zikry, M.A. (2003). Evolution of Failure Mechanisms in 2D and 3D Woven Composite Systems under Quasi-static Perforation, *J. Compos. Mater.*, **37**(18): 1651–1674.

Bazant, Z.P., Belytschko, T.B. and Chang, T.P. (1984). Continuum Theory for Strain Softening, *J. Eng. Mech.*, **110**(12): 1666–1691.

Benssousan, A., Lions, J.L. and Papanicolaou, G. (1978). *Asymptotic Analysis for Periodic Structures*, North-Holland, Amsterdam.

Buannic, N. and Cartraud, P. (2001). Higher-order Effective Modeling of Periodic Heterogeneous Beams. II. Derivation of the Proper Boundary Conditions for the Interior Asymptotic Solution, *Int. J. Solid Struct.*, **38**(40–41): 7163–7180.

Caillerie, D. (1984). Thin Elastic and Periodic Plates, *Math. Meth. Appl. Sci.*, **6**(3): 159–191.

Cioranescu, D. and Donato, P. (1999). An introduction to Homogenization, Vol. 17 of *Oxford Lecture Series in Mathematics and its Applications*, Oxford, UK, Oxford Univ. Press.

Cioranescu, D. and Saint Jean Paulin, J. (1999). *Homogenization of Reticulated Structures*, Berlin, Springer.

Courant, R. and Hilbert, D. (1989). *Methods of Mathematical Physics*, Vol. I, New York, NY, Wiley-Interscience.

Dauge, M., Gruais, I. and Rossle, A. (2000). The Influence of Lateral Boundary Conditions on the Asymptotics in thin Elastic Plates, *SIAM J. Math. Anal.*, **31**(2): 305–345.

de Borst, R. and Muhlhaus, H.B. (1992). Gradient Dependent Plasticity: Formulation and Algorithmic Aspects, *Int. J. Numer. Meth. Eng.*, **35**(3): 521–539.

de Borst, R. and Sluys, L.J. (1991). Localization in Cosserat Continuum Under Static and Dynamic Loading Conditions, *Comput. Methods Appl. Mech. Eng.*, **90**(1–3): 805–827.

Dvorak, G.J. and Benveniste, Y. (1992). On Transformation Strains and Uniform Fields in Multiphase Elastic Media, *Proc. R. Soc. Lond. A*, **437**(1900): 291–310.

Feyel, F. and Chaboche, J.-L. (2000). Fe2 Multiscale Approach for Modelling the Elastoviscoplastic Behavior of Long fiber sic/ti Composite Materials, *Comput. Methods Appl. Mech. Eng.*, **183**(3–4): 309–330.

Garcia-Castillo, S.K., Sanchez-Saez, S., Barbero, E. and Navarro, C. (2006). Response of Pre-loaded Laminate Composite Plates Subject to High Velocity Impact, *J. Phys. IV*, **136**(8): 1257–1263.

Gregory, R.D. and Wan, F.Y.M. (1984). Decaying States of Plane-strain in a Semi-infinite Strip and Boundary-conditions for Plate-theory, *J. Elasticity*, **14**(1): 27–64.

Kohn, R.V. and Vogelius, M. (1984). A New Model for Thin Plates with Rapidly Varying Thickness, *Int. J. Solids Struct.*, **20**(4): 333–350.

Kolpakov, A.G. (1991). Calculation of the Characteristics of Thin Elastic Rods with a Periodic Structure, *PMM J. Appl. Math. Mech.*, **55**(3): 358–365.

Krajcinovic, D. (1996). *Damage Mechanics*, Series in Applied Mathematics and Mechanics, North Holland, Amsterdam.

Lewinski, T. and Telega, J.J. (2000). *Plates, Laminates and Shells: Asymptotic Analysis and Homogenization*, Singapore, World Scientific.

Michel, J.C. and Suquet, P. (2004). Computational Analysis of Nonlinear Composite Structures using the Nonuniform Transformation Field Analysis, *Comput. Meth. Appl. Mech. Eng.*, **193**(48–51): 5477–5502.

Miller, R. (1994). The Eigenvalue Problem for a Class of Long, Thin, Elastic Structures with Periodic Geometry, *Q. Appl. Math.*, **52**(2): 261–282.

Needleman, A. (1988). Material Rate Dependence and Mesh Sensitivity in Localization Problems, *Comput. Meth. Appl. Mech. Eng.*, **67**(1): 69–86.

Oskay, C. and Fish, J. (2007). Eigendeformation-based Reduced Order Homogenization for Failure Analysis of Heterogeneous Materials, *Comp. Meth. Appl. Mech. Eng.*, **196**(7): 1216–1243.

Oskay, C. and Fish, J. (2008). On Calibration and Validation of Eigendeformation-Based Multiscale Models for Failure Analysis of Heterogeneous Systems, *Comp. Mech.*, **42**(2): 181–195.

Reddy, J.N. (1997). *Mechanics of Laminated Composite Plates and Shells: Theory and Analysis*, **2nd edn**, CRC Press, Boca Raton, FL.

Sanchez-Palencia, E. (1980). *Non-homogeneous Media and Vibration Theory*, Vol. 127 of *Lecture Notes in Physics*, Berlin, Springer-Verlag.

Simo, J.C. and Ju, J.W. (1987). Strain- and Stress-based Continuum Damage Models – I. Formulation, *Int. J. Solid Struct.*, **23**(7): 821–840.

Suquet, P.M. (1987). Elements of Homogenization for Inelastic Solid Mechanics. In: Sanchez-Palencia, E. and Zaoui, A. (eds), *Homogenization Techniques for Composite Media*, New York, NY, Springer-Verlag, pp. 193–278.

Tarn, J.Q. and Wang, Y.M. (1994). An Asymptotic Theory for Dynamic-Response of Anisotropic Inhomogeneous and Laminated Plates, *Int. J. Solids Struct.*, **31**(2): 231–246.

Terada, K. and Kikuchi, N. (1995). Nonlinear Homogenization Method for Practical Applications, In: Ghosh, S. and Ostoja-Starzewski, M. (eds), *Computational Methods in Micromechanics*, Vol. AMD-212/MD-62, pp. 1–16. ASME, USA.

Timoshenko, S.P. and Goodier, J.N. (1970). *Theory of Elasticity*, **3rd edn**, New York, NY, McGraw-Hill.

Trabucho, L. and Viano, J.M. (1996). Mathematical Modeling of Rods, In: Ciarlet, P.G. and Lions, J. L. (eds), *Handbook of Numerical Analysis*, Vol. 4, North Holland, Amsterdam, Elsevier.